

UNCLASSIFIED

DEL 86-U-0002

DIAGNOSTICS DEVELOPMENT FOR E-BEAM EXCITED AIR CHANNELS

Technical Report No. 3

CONDUCTIVITY MEASUREMENTS ON THE
MEDEA ELECTRON BEAM

September 27, 1985

By: M. N. Spencer, J. S. Dickinson, and D. J. Eckstrom

Sponsored by:

DEFENSE ADVANCED RESEARCH PROJECTS AGENCY
1400 Wilson Blvd.
Arlington, VA 22209

Monitored by:

OFFICE OF NAVAL RESEARCH
800 North Quincy Street
Arlington, VA 22217

DISTRIBUTION STATEMENT A
Approved for Distribution Unlimited

ARPA Order No. 4128
Contract No. N00014-84-C-0718
Effective Date: 1 June 1984
Expiration Date: 31 May 1985
Principal Investigator: D. J. Eckstrom (415) 859-4398

SRI Project PYU 7782
MP Report No. 85-220

DTIC QUALITY INSPECTED

The views and conclusions contained in this document are those of the authors and should not be interpreted as necessarily representing official policies, either expressed or implied, of the Defense Advanced Research Projects Agency or the U.S. Government.

PLEASE RETURN TO:

**BMD TECHNICAL INFORMATION CENTER
BALLISTIC MISSILE DEFENSE ORGANIZATION
7100 DEFENSE PENTAGON
WASHINGTON D.C. 20301-7100**

SRI International
333 Ravenswood Avenue
Menlo Park, California 94025-3493
(415) 326-6200
TWX: 910-373-2046
Telex: 334486

u3962

19980309 381

DEL 86-U-0002



JAN 8 1986

Accession Number: 3962

Publication Date: Sep 27, 1985

Title: Diagnostics Development for E-Beam-Excited Air Channels

Personal Author: Eckstrom, D.J.; Spencer, M.N.; Dickinson, J.S.

Corporate Author Or Publisher: SRI International, 333 Ravenswood Avenue, Menlo Park, CA 94025 Report Number: SRI PYU 7782; MP 85-220

Report Prepared for: Office of Naval Research, 800 North Quincy St., Arlington, VA 22217 Report Number Assigned by Contract Monitor: DEL 86-U-0002

Comments on Document: Archive, RRI, DEW

Descriptors, Keywords: Diagnostics Development E-beam Excite Air Channel Plasma Microwave PHERMEX Accelerator Medea Parameter Afterglow Conductivity Kinetics Benzene Photoionization Water Vapor

Pages: 00044

Cataloged Date: Nov 30, 1992

Contract Number: N00014-84-C-0718

Document Type: HC

Number of Copies In Library: 000001

Record ID: 25363

Source of Document: DEW

REPORT DOCUMENTATION PAGE

1a. REPORT SECURITY CLASSIFICATION Unclassified		1b. RESTRICTIVE MARKINGS N/A		
2a. SECURITY CLASSIFICATION AUTHORITY DARPA-CG-55		3. DISTRIBUTION/AVAILABILITY OF REPORT Approved for public release; distribution unlimited.		
2b. DECLASSIFICATION/DOWNGRADING SCHEDULE N/A				
4. PERFORMING ORGANIZATION REPORT NUMBER(S) MP 85-220		5. MONITORING ORGANIZATION REPORT NUMBER(S)		
6a. NAME OF PERFORMING ORGANIZATION SRI International	6b. OFFICE SYMBOL (If applicable)	7a. NAME OF MONITORING ORGANIZATION Office of Naval Research		
6c. ADDRESS (City, State and ZIP Code) 333 Ravenswood Avenue Menlo Park, CA 94025		7b. ADDRESS (City, State and ZIP Code) 800 North Quincy Street Arlington, VA 22217		
8a. NAME OF FUNDING/SPONSORING ORGANIZATION Defense Advanced Research Projects Agency	8b. OFFICE SYMBOL (If applicable)	9. PROCUREMENT INSTRUMENT IDENTIFICATION NUMBER Contract No. N00014-84-C-0718		
8c. ADDRESS (City, State and ZIP Code) 1400 Wilson Boulevard Arlington, VA 22209	10. SOURCE OF FUNDING NOS.			
	PROGRAM ELEMENT NO. 4128	PROJECT NO. Amendment 9	TASK NO.	WORK UNIT NO.
11. TITLE (Include Security Classification) Conductivity Measurements on the Medea Electron Beam				
12. PERSONAL AUTHOR(S) M.N. Spencer, J.S. Dickinson, D.J. Eckstrom				
13a. TYPE OF REPORT Technical	13b. TIME COVERED FROM _____ TO _____	14. DATE OF REPORT (Yr., Mo., Day) 1985 Sept. 27	15. PAGE COUNT 44	
16. SUPPLEMENTARY NOTATION				
17. COSATI CODES		18. SUBJECT TERMS (Continue on reverse if necessary and identify by block number)		
FIELD	GROUP			SUB. GR.
19. ABSTRACT (Continue on reverse if necessary and identify by block number)				
<p>Afterglow conductivity decay measurements were performed on the Medea electron beam at pressures from 1 to 50 torr in dry and laboratory air and in neon at 100 torr. Most measurements were made using the microwave cavity perturbation technique, which is sensitive to conductivities in the range of approximately 10^6 to 10^8 sec^{-1}. Two conditions were also studied using a 35-GHz microwave interferometer, which is sensitive in the range of 10^9 to 10^{11} sec^{-1}.</p> <p>The results are in reasonable agreement with our previous measurements made using excitation by a Febetron 706 electron beam. The absence of a quartz tube around the beam in the Medea experiments led to slightly longer conductivity decays at pressures below 10 torr, where charge decay is governed by ambipolar diffusion.</p>				
20. DISTRIBUTION/AVAILABILITY OF ABSTRACT UNCLASSIFIED/UNLIMITED <input checked="" type="checkbox"/> SAME AS RPT. <input type="checkbox"/> DTIC USERS <input type="checkbox"/>		21. ABSTRACT SECURITY CLASSIFICATION Unclassified		
22a. NAME OF RESPONSIBLE INDIVIDUAL C. M. Huddleston	22b. TELEPHONE NUMBER (Include Area Code) (202) 394-1264	22c. OFFICE SYMBOL N60921		

The Medea decays were also slightly longer at 20 and 50 torr, which we believe is partly due to the density reduction in the channel caused by hydrodynamic expansion and partly caused by the higher levels of electron beam excitation in the Medea experiments compared to the Febetron experiments. In a double pulse experiment in 50-torr laboratory air, the afterglow decay from the second pulse was about 30% longer than from the first pulse, which could again be due to a second reduction in channel density caused by the second pulse.

The DC conductivities at 200 to 500 μs after the first pulse can be extrapolated from our measurements to fall in the $(1 \text{ to } 4) \times 10^8 \text{ sec}^{-1}$ range for air pressures in the 4 to 20 torr range, depending on the humidity of the air. This is the range of conductivities predicted to optimize channel tracking for the Medea beam. McDonnell-Douglas experiments to date do show the best channel tracking at 4 to 8 torr, in agreement with these conductivity measurements and the theoretical predictions.

ACKNOWLEDGMENTS

We are grateful for the cooperation and generous assistance of Evan Rose, Carl Leader, Edward Theby, Ken Thiele, and Frank Bieniosek of the McDonnell-Douglas Research Laboratory staff in performing these measurements.

CONTENTS

	ACKNOWLEDGMENTS.....	iii
	LIST OF ILLUSTRATIONS.....	v
I	INTRODUCTION.....	1
II	EXPERIMENTAL.....	3
	MEDEA Accelerator.....	3
	Microwave Diagnostics.....	3
	Test Gases.....	4
III	RESULTS.....	6
IV	DISCUSSION.....	10
	Summary and Comparison of Results.....	10
	Implications for Channel Tracking.....	11
	Decay Rates.....	11
	Identity of the Charge Carrier.....	13
	Double-Pulse Experiment.....	15
	Interferometer Results.....	16
V	CONCLUSIONS.....	17
VI	REFERENCES.....	18

FIGURES

1. Typical Current Traces for the Medea Double-Pulse Accelerator.....	19
2. Schematic of Microwave Cavity Experimental Setup.....	20
3. Schematic of Microwave Interferometer Experimental Setup.....	21
4. Afterglow Conductivity Decay Histories for 1-Torr Synthetic Air.....	22
5. Afterglow Conductivity Decay Histories for 4-Torr Synthetic Air.....	23
6. Afterglow Conductivity Decay Histories for 8-Torr Synthetic Air.....	24
7. Afterglow Conductivity Decay Histories for 20-Torr Synthetic Air....	25
8. Afterglow Conductivity Decay Histories for 50-Torr Synthetic Air....	26
9. Afterglow Conductivity Decay Histories for 4-Torr Laboratory Air ...	27
10. Afterglow Conductivity Decay Histories for 8-Torr Laboratory Air....	28
11. Afterglow Conductivity Decay Histories for 20-Torr Laboratory Air...29	
12. Afterglow Conductivity Decay Histories for 50-Torr Laboratory Air...30	
13. Afterglow Conductivity Decay Histories for 100-Torr Neon.....	31
14. Double-Pulse Afterglow Conductivity Decay Histories for 50-Torr Laboratory Air.....	32
15. Afterglow Conductivity Decay Histories for 1-Torr Laboratory Air From Interferometer Measurements.....	33
16. Afterglow Conductivity Decay Histories for 4-Torr Laboratory Air Including Interferometer Data.....	34
17. Real Conductivity Histories for Synthetic Air Excited by the Medea Electron Beam.....	35
18. Real Conductivity Histories for Laboratory Air Excited by the Medea Electron Beam.....	36
19. Real Conductivity Histories for Synthetic Air Excited by the Febetron Electron Beam.....	37
20. Real Conductivity Histories for Laboratory Air Excited by the Febetron Electron Beam.....	38
21. D.C. Conductivity Histories for Synthetic Air Excited by the Medea Electron Beam.....	39
22. D.C. Conductivity Histories for Laboratory Air Excited by the Medea Electron Beam.....	40
23. Electron Density Histories for Synthetic Air Excited by the Medea Electron Beam.....	41

24.	Electron Density Histories for Laboratory Air Excited by the Medea Electron Beam.....	42
25.	Electron Density Decay Rates in E-Beam-Excited Air.....	43
26.	Afterglow Conductivity Decay Histories for 4-Torr Laboratory Air With Corrected Interferometer Data.....	44

I INTRODUCTION

The MEDEA accelerator at McDonnell-Douglas Research Laboratory (MDRL) is the first high current electron beam source capable of generating closely spaced pulses ($\Delta t > 200 \mu\text{s}$). This has allowed the MDRL staff to study channel tracking--the effects of residual density and conductivity channels created by the first pulse on the propagation characteristics of the second pulse. Preliminary experiments have demonstrated significant differences in second pulse propagation for varying gas pressures and interpulse spacings [LR85]. The best tracking results were obtained at pressures in the 4- to 8-torr range.

Bieniosek and Rose used the laser deflection technique [GR82] to characterize the residual density channel from a single MEDEA pulse [BR85]. They measured an initial neutral density reduction of 25% at the channel centerline and a full-width-at-half-maximum of the lowered density of 2.5 cm. This low density column persisted until the weak shock wave generated in the channel formation process reflected off the propagation tank walls (I.D. = 15 cm) and returned to the channel axis at approximately 380 μs . The channel was then restored to its original density and temperature until the cycle repeated itself at $\sim 420 \mu\text{s}$. Therefore, the effects of the neutral density channel on second pulse propagation are expected to be minimized between 380 and 420 μs . It is also expected that the charge density channel would change properties in this time interval as the shock wave perturbs the plasma density, plasma diameter, electron temperature, and the electron collision frequency. However, the conductivity may not be perturbed, because it is proportional to the ratio of n_e/ν , and both of those parameters are affected equally by shock compression and expansion.

The channel conductivities expected to exist at 200 to 500 μs after a Medea pulse are in the measurement range of our microwave cavity perturbation technique [Ec83,SDE85]. Therefore, to support the MDRL two-pulse propagation studies, we performed cavity measurements at the MEDEA facility between April 11 and April 19, 1985. We also measured conductivities with a 35-GHz interferometer [EDS85] for two-channel conditions as a supplement to the cavity

measurements. Because the MEDEA beam propagates best at low air pressures, we confined our measurements to a similar low pressure range.

II EXPERIMENTAL

MEDEA Accelerator

The MEDEA accelerator uses a pair of high voltage pulse transformers to drive a pulse forming line. One transformer is used to generate the first electron pulse and the second transformer is triggered, after a preselected time delay, to generate the second pulse. Both the beam energy and current are variable. The earlier experiments cited in the previous section and the current microwave experiments were done with a beam energy of 1 MeV and current of ~ 6.5 kA. The pulse length was 8 ns and the beam diameter at the exit foil was ~ 1 cm. Typical current traces for both the first and second pulses are shown in Figure 1.

Microwave Diagnostics

Our microwave diagnostic apparatus has been described in detail in previous reports [Ec83,SDE85,EDS85]. The microwave cavity was designed to operate on the TM_{010} mode at 1.65 GHz. It was mounted in the beam line 43 cm from the exit foil as shown in Figure 2. For each test gas condition, we recorded histories of the cavity transmission, using a Tektronix R7912 transient digitizer, at frequency intervals of 200 KHz. A total of approximately 50 shots was taken in each case, with about 1 minute between each shot. Transforming the time-dependent data to frequency-dependent data was done by computer analysis and yielded a set of transmission profiles for the cavity at various times in the afterglow. The computer-generated parameters for these profiles were then used to compute the real and imaginary conductivities as a function of afterglow time. We used the constant electron collision frequency approximation to calculate the momentum-transfer collision frequency. With the additional assumption that the charge density is dominated by the electron density, we also found values for this latter parameter.

Open-shutter photographs of the electron beam indicated that the electron beam was attenuated as it passed through the cavity. Faraday cup measurements made 70 cm downstream from the exit foil gave a peak current of 2 kA with the

cavity in place, compared with an initial beam current of 6.5 kA. The cavity therefore perturbs the beam, most likely by physically obstructing the wings of the beam's 2.8-cm-diameter Bennett profile [BR85] at the 2.5-cm-diameter entrance of the cavity. (This is calculated to cause a loss of 57% of the beam current, compared with the measured loss of 70%.) This apparent clipping of the beam did not interfere with the microwave measurements. We analyzed the data assuming a beam diameter (and hence a plasma diameter) of 2.5 cm. Conductivity measurements thus represent average values over this cross-sectional area.

For the microwave interferometer measurements, the probe beam was located 39 cm downstream from the foil, as shown in Figure 3. We used the same "pseudo-horn" system that was used in the PHERMEX experiments at Los Alamos National Laboratories [EDS85]. In this configuration the waveguide flares in the E-plane from its normal height of 0.36 cm to 3.2 cm, while the width in the H-plane is held constant at 0.71 cm. The H-plane walls were removed at the tank center-line to create an aperture that measures 2.5 cm wide and 3.2 cm high, through which the electron beam passes. Because the microwave power is uniform to within 20% over the entire rectangular aperture, the conductivity measured using the interferometer is also an average over this area.

Test Gases

Measurements in our own laboratory using Febetron 706 excitation showed that the conductivity decay in laboratory air is much faster than in synthetic air (80% nitrogen, 20% oxygen) [SDE85]. Further experiments confirmed that this is due to the presence of water vapor in the laboratory air. We therefore studied both types of air. We measured the humidity in MEDEA's propagation tank for laboratory and synthetic air at each of the pressures studied. For synthetic air, the water vapor content, presumably originating from water in the supply tank and flow line, varied from approximately 0.016 to 0.15 torr as the air pressure varied from 1 to 50 torr. The water vapor pressure in the laboratory air over this range varied from approximately 0.08 to 2.8 torr. As in our experiments at SRI, we found that the mole fraction of water in the propagation tank was greater than that in ambient air (i.e., at atmospheric pressure). Presumably this occurs because of the different pumping efficiencies between nitrogen or oxygen and water. Our humidity measurements are

uncertain because the calibration of the hygrometer (Ondyne Model 1461) changed during the running of the experiments. Because we prevent electron impingement on the semiconductor probe surface, this must be an x-ray effect. An additional uncertainty in the water vapor pressure measurements arose from the very long time (>1 hour) needed for the propagation tank and/or probe to equilibrate to a new water vapor pressure when the gas pressure was changed.

Our first measurements were made on a static fill of 8 torr dry air. During the approximately 50 shots required to make a complete conductivity measurement, the conductivity decay rate increased. This is symptomatic of impurities in the test gas caused either by desorption of contaminants from the walls (possibly aided by electron beam impingement) or by products of the ionization reactions in air. To remove this source of error, we continuously flowed the test gas through the propagation tank in all subsequent experiments.

In addition to dry and laboratory air studies, we also made conductivity measurements on neon at 100 torr to support anticipated propagation experiments at that condition.

III RESULTS

Microwave cavity measurements were performed on synthetic air at five pressures: 1, 4, 8, 20, and 50 torr. With the exception of 1 torr, these measurements were repeated on laboratory air. Because of time constraints, we were able to perform interferometer measurements at only 1 and 4 torr of laboratory air. The water vapor pressure measurements for these tests are presented in the form of partial pressures in Table 1.

The data analysis methods for both the cavity and the interferometer have been described in detail in previous reports [SDE85,EDS85]. Basically, both techniques allow an attenuation and a phase shift measurement for the microwave probe beam; these measurements can be interpreted as real and imaginary conductivities, σ_r and σ_i . These two parameters can be used to calculate the momentum-transfer collision frequency, ν , and the plasma frequency, ω_p (see below). With the usual assumption that the conductivity is due solely to electrons, the plasma frequency can be used to calculate the electron density. The further assumption that the electron energy distribution is Maxwellian allows deduction of the electron temperature from the collision frequency.

Figures 4 through 13 show results from the microwave cavity experiments, consisting of the time dependence of the real conductivity (σ_r), the DC limit of the real conductivity (σ_{DC}), the collision frequency under the constant collision frequency approximation (ν), and the electron density (n_e) (also calculated using the same approximation). The real conductivity, which is measured directly in the experiments, is defined as

$$\sigma_r = \epsilon_0 \omega_p^2 \nu / (\nu^2 + \omega^2)$$

where ω is the microwave angular frequency. σ_r will depend on the microwave measurement frequency unless $\nu \gg \omega$, in which case the conductivity goes over to the DC-limiting value

Table 1

Water Content in Test Gases

<u>P_{total} (torr)</u>	<u>Synthetic Air P_{H₂O} (torr)</u>	<u>Laboratory Air P_{H₂O} (torr)</u>
1	0.016	-
4	0.016	0.018
8	0.061	0.473
20	0.135	1.63
50	0.150	2.76

$$\sigma_{DC} = \epsilon_0 \omega_p^2 / \nu$$

If we assume that electrons are the sole charge carriers, then

$$\omega_p^2 = n_e e^2 / m_e \epsilon_0 .$$

In the constant-collision-frequency approximation, the collision frequency is related to the measured real and imaginary conductivities as

$$\nu = -\omega \sigma_r / \sigma_i .$$

The DC conductivity can be used to compare conductivity measurements at different frequencies (e.g., the cavity and interferometer measurements), and also is of intrinsic interest in propagation analyses. We therefore use the measured collision frequencies to calculate σ_{DC} from σ_r .

The results reported above were made with the MEDEA accelerator operating in the single-pulse mode. We also made one measurement in 50-torr laboratory air using double-pulse operation to compare the afterglow decays following the first and second pulses. The pulses in these tests were spaced 250 μ s apart. To compare conductivity and electron density histories over the same relative time scale for each pulse, we have plotted the results in Figure 14 on a linear time scale. Careful comparison shows that the absolute values of conductivity and electron density are slightly higher at comparable times after the second pulse than after the first, and that the decay rates are slightly slower.

As noted above, we also measured the afterglow conductivity in 100 torr of neon. The electron attachment rate in neon is essentially zero, so the conductivity decay in the late afterglow must depend on electron-ion recombination, which gets progressively slower as the charge density decreases. Thus, we expect the conductivity decay to be rather long in the range of the cavity measurement, and this is indeed the case as demonstrated by the results presented in Figure 13. Even after 10 ms, the conductivity and electron density have decayed only to the middle of the cavity range of sensitivity. Unfortunately, the digitizer is not capable of recording at a slower time

scale and we were therefore unable to measure the conductivity decay over the complete range of sensitivity of the cavity.

We obtained interferometer data for only two conditions: 1 torr and 4 torr of laboratory air. These results are shown in Figures 15 and 16, together with the corresponding results obtained with the microwave cavity. In contrast to the cavity experiments, the interferometer method requires only one electron beam pulse to yield a complete time history. Because it operates at a higher microwave frequency than the cavity, and because it is a single-pass measurement rather than a standing-wave measurement, the interferometer is sensitive to higher conductivities than the cavity. Thus, the interferometer data are recorded earlier in the afterglow than the cavity data, and extend both the time range and the range of magnitude of conductivity for the measurements.

IV DISCUSSION

Summary and Comparison of Results

Figures 17 and 18 summarize the conductivity decay time histories for synthetic air and laboratory air, respectively, at each pressure studied. For comparison, Figures 19 and 20 present the same information for our Febetron experiments [SDE85]. In both the synthetic and laboratory air cases, the Medea results for pressures below 10 torr show conductivity decays that are two to four times longer than the corresponding results from the Febetron. The 50-torr data in both cases are consistent with the Febetron data, falling midway between the 30- and 100-torr results. The 20-torr Medea data also fall midway between the 10- and 30-torr Febetron data at the beginning of the measured decays, but the Medea decays become longer at later times.

We attribute the differences between Medea and Febetron results at low pressures to the fact that the Febetron experiments were conducted with a 2.5-cm-diameter quartz tube passing through the cavity via the holes in the endwalls to enclose and define the plasma column, whereas in the Medea experiments the cavity flanges were sealed directly to the 15-cm-diameter propagation tank (Figure 2). The plasma decay at low pressures ($p < 10$ torr) is primarily due to ambipolar diffusion (see below), which reduces the charge density in the central part of the cavity, where the sensitivity is highest, and also moves charges to the walls where recombination can take place. The presence of walls at 1.2-cm radius in the Febetron experiments caused recombination to occur sooner in those experiments, which accounts for the shorter decays compared to the Medea experiments.

We have been concerned that the walls of the quartz tube also might have interfered with our Febetron data directly through a contribution to the conductivity from the quartz irradiated by the electron beam. The essential agreement between Medea and Febetron results indicates that such an effect cannot be very large.

Implications for Channel Tracking

According to simple theory [BL84], the optimum DC conductivity for channel tracking is approximately

$$4\pi \sigma_{DC} a/c = 0.1 \quad ,$$

where a is the beam radius and c is the speed of light. For the parameters of the Medea accelerator, this optimum value is about $2.5 \times 10^8 \text{ sec}^{-1}$. Figure 21 presents a summary of the time histories of σ_{DC} for synthetic air at the five pressures tested. We have also outlined the range of predicted conductivities for tracking (predicted value multiplied and divided by 2) and the range of delay times for the second pulse used in the MDRL tracking experiments. Although our experiments do not specifically include the area of the σ_{DC} -time envelope expected for channel tracking, it appears from simple extrapolation that the conductivities should have been in the desired range for pressures in the 8 to 20 torr range. The experimental observation that optimum second-pulse propagation occurred at 4 to 8 torr [LR85] may indicate that the desired residual channel conductivity is somewhat higher than predicted by the above equation. Alternately, the air in the cell during the channel tracking experiments may not have been as dry as for these synthetic air conductivity experiments. As indicated in Figure 22, the DC conductivities for 4 and 8 torr laboratory air are approximately $2 \times 10^8 \text{ sec}^{-1}$ at 200 to 500 μs after the first pulse. Thus, it is important to know the test conditions quite accurately to achieve a definitive comparison of experiment and theory.

Decay Rates

We can compare our results in more detail and evaluate them in terms of simple air chemistry by examining the charge-density decay rates as a function of pressure and gas composition. The first point to emphasize is that our measurements are made rather late in the afterglow. We estimate that the electron density in the air channel during the e-beam pulse is in the 10^{13} to $10^{14}/\text{cm}^3$ range, whereas the microwave cavity is sensitive to electron densities in the 10^7 to $10^{10}/\text{cm}^3$ range. Immediately after termination of the pulse, the charge density is rapidly reduced by electron-ion recombination. At the lower electron densities characteristic of our measurements, the

electron density decay is governed by electron attachment, or, at pressures below 10 torr, by ambipolar diffusion. Because electron attachment is first order in electron density, the decay is expected to be exponential. Likewise, for the range of diffusion coefficients appropriate for air plasmas, one can show that ambipolar diffusion decay should be approximately exponential [SDE85]. Therefore, we have fit our electron density data to exponentials, using a least-squares fitting routine, and have determined the decay rates from the fits. The electron density decay histories for synthetic and laboratory air are presented in Figures 23 and 24, respectively, together with the curve fits. The resulting decay rates are presented in Figure 25, together with similar results from our previous Febetron experiments [SDE85].

As in our previous experiments we see a decrease in the decay rates when the pressure is raised from 1 torr to 8 torr in both synthetic and laboratory air. As noted above, we attribute this effect to the dominance of ambipolar diffusion decay, with the diffusion coefficient decreasing with pressure. The decrease does not follow a p^{-1} dependence one would expect for a pure diffusion process, because chemical reactions become increasingly important as the gas pressure rises. We noted above the differences in geometry between the Medea and Febetron experiments; the absence of a quartz tube in the former case increases the effective path length for diffusion and therefore decreases the diffusional loss rates as observed in Figure 25.

At pressures greater than 8 torr, the electron density decay rates increase with increasing pressure for both synthetic and laboratory air samples. The variation of decay rate with pressure appears to be approaching a p^2 dependence at high pressures, as was the case in our previous data. Such a pressure dependence is consistent with electron attachment being the dominant electron decay pathway in this pressure range, although absolute values of the decay rates are smaller than expected for electron attachment [SDE85]. As in our Febetron experiments, the conductivity and electron density decay rates for laboratory air were significantly higher than those for synthetic air. We have demonstrated that this effect is due to water vapor [SDE85].

The present Medea decay rates are slightly slower than the rates from the Febetron experiments for comparable pressures, even though our humidity measurements indicate that the water vapor pressures were somewhat higher in the Medea tests than in the Febetron tests. The differences may be due to the

presence or absence of the quartz tube in the experiment, but they are more likely due to two other effects. First, we must remember that the Medea beam deposits sufficient energy in the air channel to heat it significantly, which leads to a hydrodynamic expansion and subsequent density channel formation, reported to consist of a 25% density reduction [BR85]. Assuming an isentropic expansion from the initial hot, but unexpanded channel, this corresponds to a channel temperature of 450 K before expansion and 400 K after expansion. If the conductivity decays are governed by electron attachment, their effective rates should vary as $(\text{density})^2(\text{temperature})^{1/2}$, which corresponds to a 35% reduction of the decay rate compared to a cold (300 K) channel at the same initial pressure. This only partly explains the difference in rates between the Medea and Febetron data.

The second effect is related to the initial level of excitation by the electron beams. The Medea beam total charge was more than four times the Febetron total charge. (Both have comparable peak currents and beam sizes at the foil exit, but the Medea pulse is four times longer and the Febetron beam expands and dissipates on the tube walls as it propagates downstream through the microwave cavity.) We suggest that the late-time charge decays become progressively longer than the electron-attachment decay times as the initial excitation density increases.

Identity of the Charge Carrier

In previous reports [Ec83,SDE85], we suggested that the conductivities measured in the late afterglows of e-beam ionized air at higher pressures for synthetic or laboratory air, and perhaps at all pressures for lab air, were due to negative ions rather than to electrons. This argument was advanced for two reasons. First, model calculations of the time-dependent electron density show that it drops below the measureable level (10^7 cm^{-3}) in a few microseconds for pressures above 100 torr. We, however, measure conductivity levels to times as long as several milliseconds. Second, calculations of the electron momentum-transfer collision frequency based on known collision cross sections of electrons with nitrogen, oxygen, and water molecules as a function of electron temperature yield a range of allowable collision frequencies. In particular, there is a minimum collision frequency for electron temperatures greater than or equal to room temperature. (The minimum value increases

rapidly with increasing water vapor pressure.) Collision frequencies deduced from our laboratory air Febetron data, however, were all lower than the minimum calculated values. The lower momentum-transfer collision frequencies are consistent with values for negative ions [Ec83].

This latter observation is again the case in the current Medea laboratory air data. The minimum collision frequency that one ought to observe in an air sample containing a water mole fraction of approximately 6% is $1 \times 10^{12} \text{ sec}^{-1} \text{ amagat}^{-1}$ (normalized to one atmosphere pressure), whereas the range that we measure is $(2.5-5) \times 10^{11} \text{ sec}^{-1} \text{ amagat}^{-1}$. This again implies that the charge carriers in the laboratory air experiments were negative ions rather than electrons.

The conductivities measured with microwave diagnostic techniques are correct regardless of the identity of the charge carriers. (In fact, they are the sum of conductivities from electrons and ions.) The momentum-transfer collision frequencies and plasma frequencies deduced from the conductivities are also correct. In the data presentation, we assume that the plasma frequencies are due to electrons and assign electron number densities accordingly, but the plasma frequencies could equally well be due to negative ions. In the latter case, the negative ion concentrations would be higher than the calculated electron densities by the mass ratio $m_{\text{ion}}/m_{\text{electron}}$, which is of order 10^5 .

There are two difficulties with this assignment of measured conductivities to negative ions. First, the density of negative ions must exceed that of electrons by the mass ratio for the ion contribution to dominate. Because the calculated electron densities range from 10^7 to $10^{10}/\text{cm}^3$, this requires ion densities of 10^{12} to $10^{15}/\text{cm}^3$. However, this is comparable to or larger than the total charge density initially created by the electron beam, and it is improbable that a high fraction of the initial electrons attach to form negative ions at the low pressures of these experiments. (Electron-ion recombination should dominate over electron attachment until $n_e < 2 \times 10^{12}/\text{cm}^3$ for $p < 50$ torr with 6% water vapor in air.) Secondly, if the measured conductivities are due to negative ions, then the charge density decay should be governed by ion-ion recombination rather than by electron attachment. Recombination leads to a t^{-1} dependence of the charge density, rather than to an exponential dependence, which should give a pronounced concave upward shape to

the decay curves of Figure 23. Thus, there is some inconsistency in assigning the conductivities to negative ions.

Double-Pulse Experiment

In contrast to the single pulse data presented in Figures 4 through 13 on log-log plots, the double pulse results at 50-torr laboratory air were presented in Figure 14 on a linear time scale. This facilitates visual comparison of the afterglow plasma properties following the first and second pulses. The decays appear quite similar, but a detailed comparison shows that at 50 μ s after each pulse, σ and n_e are about a factor of two higher after the second pulse than after the first. Furthermore, the decays are slower for the second pulse than for the first, so that the ratios of σ and n_e following the first and second pulses steadily increase at later times. There is also some upward curvature in the n_e versus t plot for the second pulse, which suggests ion-ion recombination as described above.

This is the first demonstration of a multiple pulse afterglow conductivity measurement, and it is interesting that such a pronounced effect was observed. In fact, it might be considered surprising, since the residual charge density at the initiation of the second pulse was less than 10^8 electrons/cm³ or 10^{13} ions/cm³ (depending on the identity of the charge carriers), whereas the beam pulse creates more than 10^{14} charges/cm³. However, just as the first pulse creates a higher temperature, reduced density channel that should reduce the decay time, the second pulse should further increase the temperature and reduce the channel density. Thus, we expect the decay from the second pulse to be longer than that from the first. If the reduction in the decay rate for the second pulse is the same as the 35% we predicted for the first pulse, it accounts for the observed difference. We also suggested above that afterglow decays are longer as the energy deposited by the beam increases (although we would expect that the energy would have to be deposited in a single pulse, or at least within a maximum time). We cannot distinguish between causes; an understanding of these observations requires detailed air chemistry calculations coupled with hydrodynamic expansion calculations. However, it is clear that measurements like these are very important in multiple pulse experiments.

Interferometer Results

In the discussion above, we have not referred specifically to the interferometer data, both because it is very limited and because it appears to be less reliable than the cavity data. This is exhibited in part by the comparison with the cavity data at 4 torr (Figure 16), which shows discontinuities in all the parameters; the collision frequency, in particular, is unrealistically high. In our analysis of similar experiments conducted on the PHERMEX accelerator at Los Alamos, we concluded that the microwave probe beam was suffering some other loss in addition to plasma absorption as it passed through the pseudo-horn probe system, most likely due to refraction by the cylindrical plasma created by the electron beam [EDS85]. In analyzing those data, we devised a correction to the interferometer data based on the assumption that the collision frequency should be equal to the average value measured in the cavity experiment at the same pressure [EDS85]. We have applied this same correction to the data at 4 torr, with the results shown in Figure 26. We cannot correct the 1 torr data because we do not have cavity data at that condition.

With this correction, the DC conductivities and the electron densities are in good agreement for the interferometer and cavity results. Between them, they cover nearly five orders of magnitude. We do not expect the values of σ_r to form a smooth variation between the two measurements because the $v/(v^2 + \omega^2)$ term in the definition of that parameter is substantially different at the two different microwave frequencies.

V CONCLUSIONS

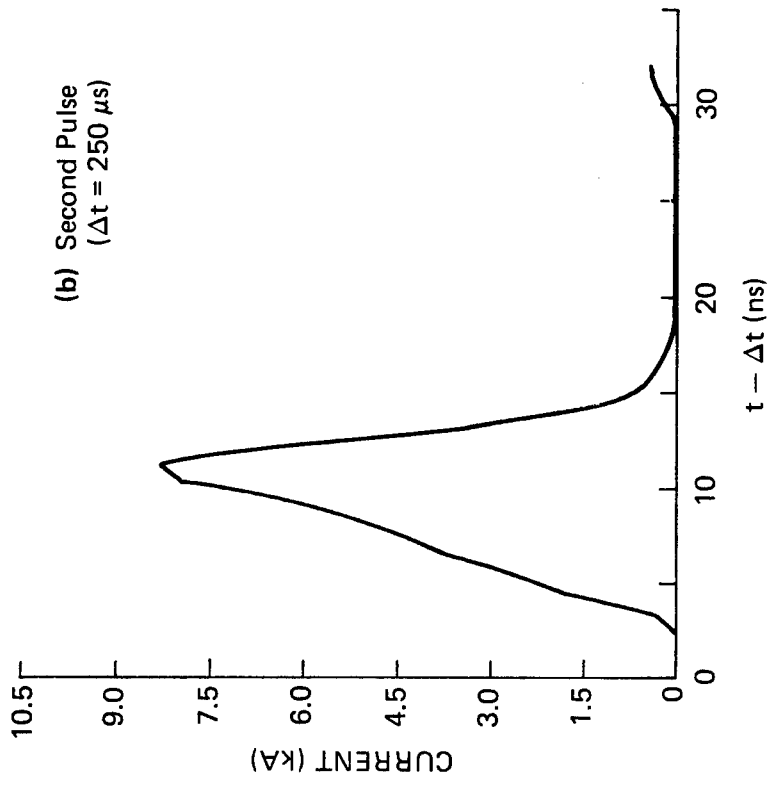
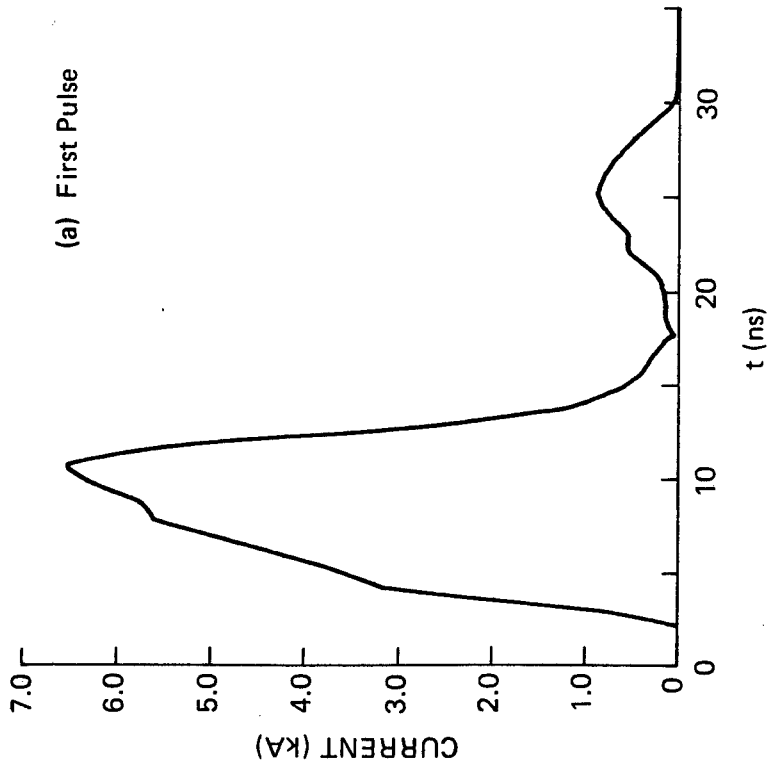
Afterglow conductivity decay measurements were performed on the Medea electron beam at pressures from 1 to 50 torr in dry and laboratory air and in neon at 100 torr. Most measurements were made using the microwave cavity perturbation technique, which is sensitive to conductivities in the range of approximately 10^6 to 10^8 sec^{-1} . Two conditions were also studied using a 35-GHz microwave interferometer, which is sensitive in the range of 10^9 to 10^{11} sec^{-1} .

The results are in reasonable agreement with our previous measurements made using excitation by a Febetron 706 electron beam. The absence of a quartz tube around the beam in the Medea experiments led to slightly longer conductivity decays at pressures below 10 torr, where charge decay is governed by ambipolar diffusion. The Medea decays were also slightly longer at 20 and 50 torr, which we believe is partly due to the density reduction in the channel caused by hydrodynamic expansion and partly caused by the higher levels of electron beam excitation in the Medea experiments compared to the Febetron experiments. In a double pulse experiment in 50-torr laboratory air, the afterglow decay from the second pulse was about 30% longer than from the first pulse, which could again be due to a second reduction in channel density caused by the second pulse.

The DC conductivities at 200 to 500 μs after the first pulse can be extrapolated from our measurements to fall in the $(1 \text{ to } 4) \times 10^8$ sec^{-1} range for air pressures in the 4 to 20 torr range, depending on the humidity of the air. This is the range of conductivities predicted to optimize channel tracking for the Medea beam. McDonnell-Douglas experiments to date do show the best channel tracking at 4 to 8 torr, in agreement with these conductivity measurements and the theoretical predictions.

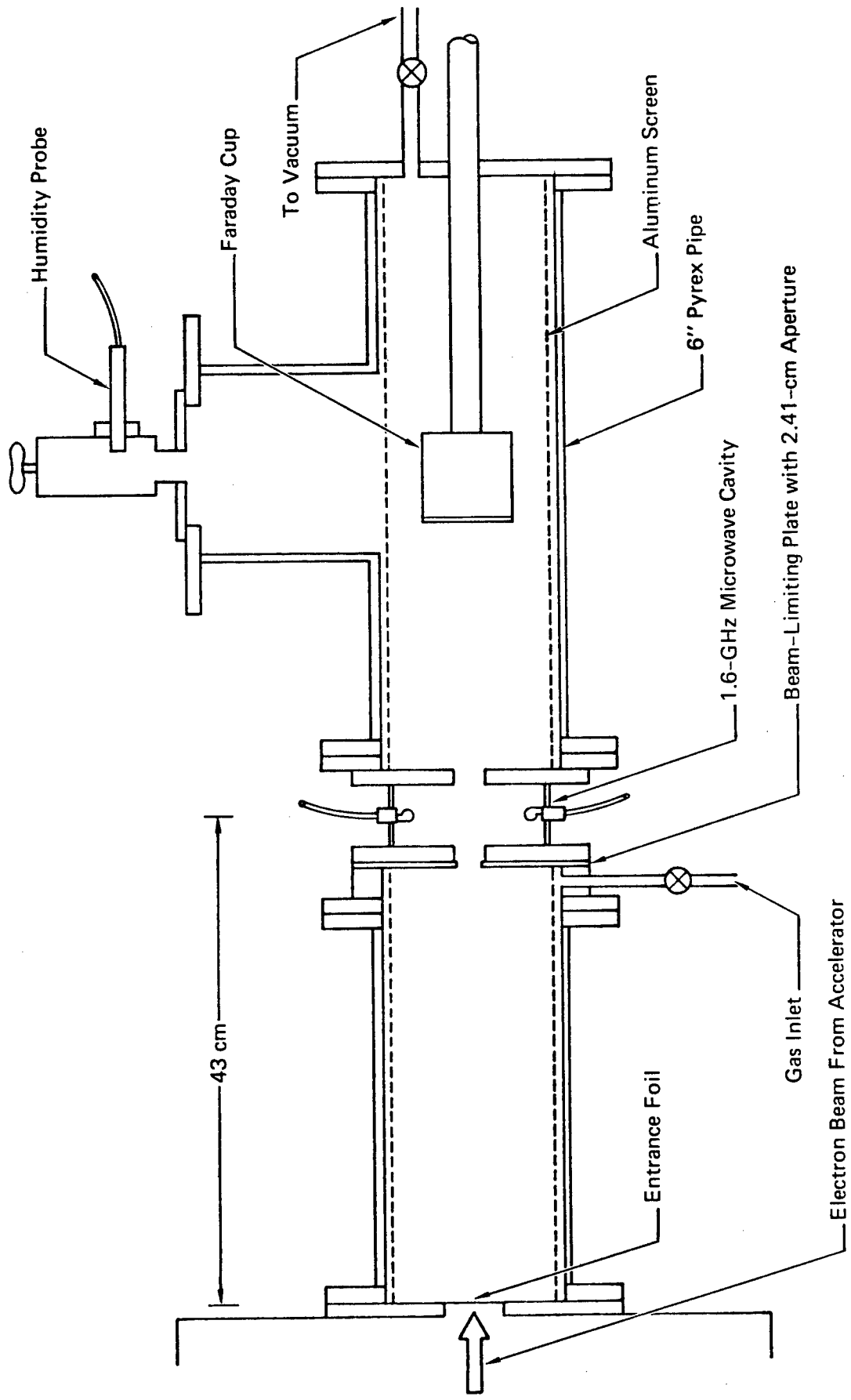
VI REFERENCES

- BL84 B. Hui and M. Lampe, Naval Research Laboratory (quoted by J. C. Leader, McDonnell-Douglas Research Laboratories, private communication).
- BR85 F. Bieniosek and E. A. Rose, McDonnell-Douglas Research Laboratories (private communication).
- Ec83 D. J. Eckstrom, "Diagnostics Development for E-Beam Excited Air Channels, Conductivity Measurements in Air Afterglows," Semiannual Technical Report No. 2, Contract N00014-81-C-0208, SRI International (March 1983).
- EDS85 D. J. Eckstrom, J. S. Dickinson, and M. N. Spencer, "Diagnostics Development for E-Beam Excited Air Channels, Conductivity Measurements on the PHERMEX Electron Beam," Technical Report No. 2, Contract N00014-84-C-0718, SRI International (July 1985).
- GR82 M. A. Greenspan and K. V. Reddy, Appl. Phys. Lett., 40, 576 (1982).
- LR85 J. C. Leader and E. A. Rose, McDonnell-Douglas Research Laboratories (private communication).
- SDE85 M. N. Spencer, J. S. Dickinson, and D. J. Eckstrom, "Diagnostics Development for E-Beam Excited Air Channels, Afterglow Conductivity Studies of the Febetron Electron Beam," Technical Report No. 1, Contract No. N00014-84-C-0718, SRI International (July 1985).



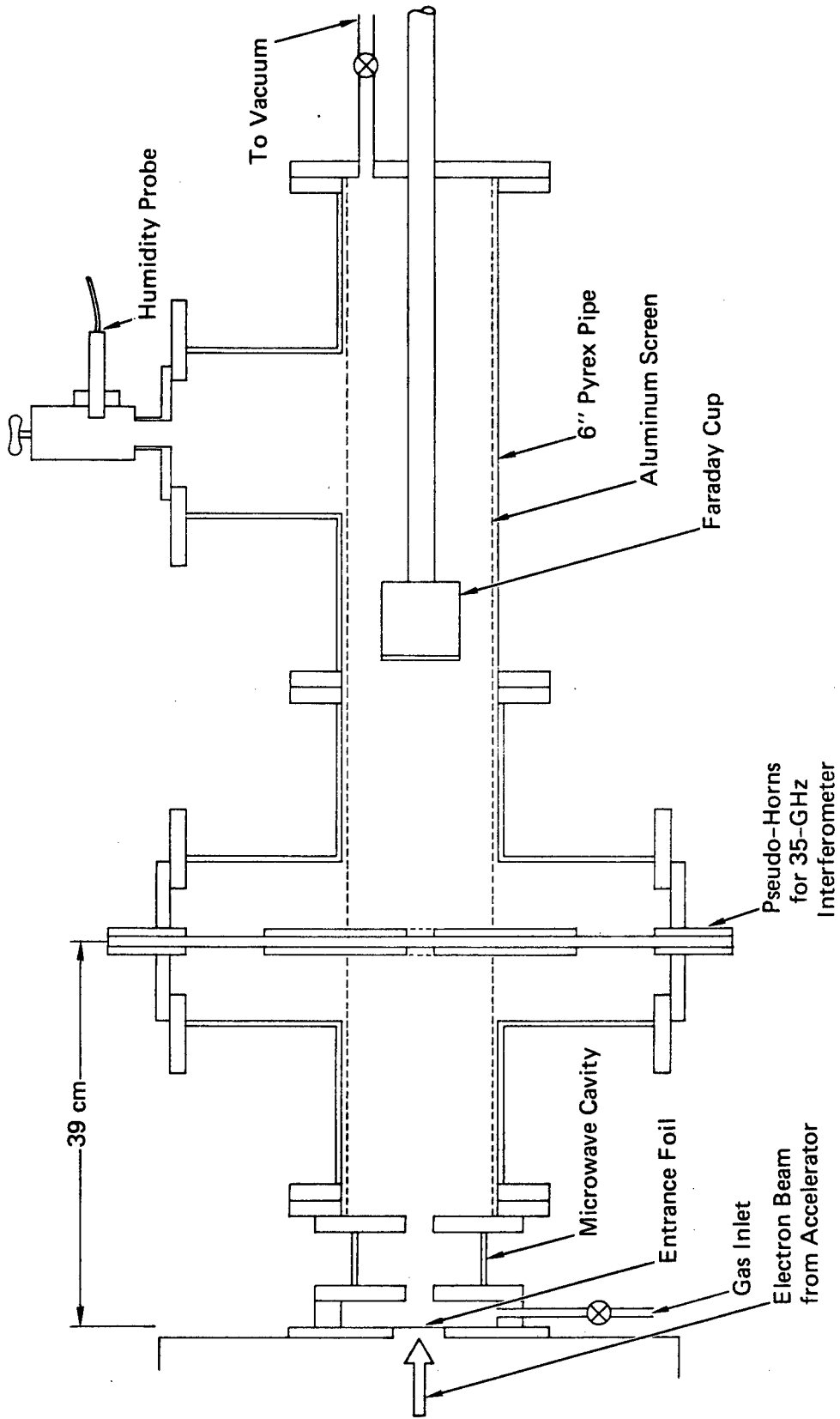
JA-8849-79

FIGURE 1 TYPICAL CURRENT TRACES FOR THE MEDEA DOUBLE-PULSE ACCELERATOR



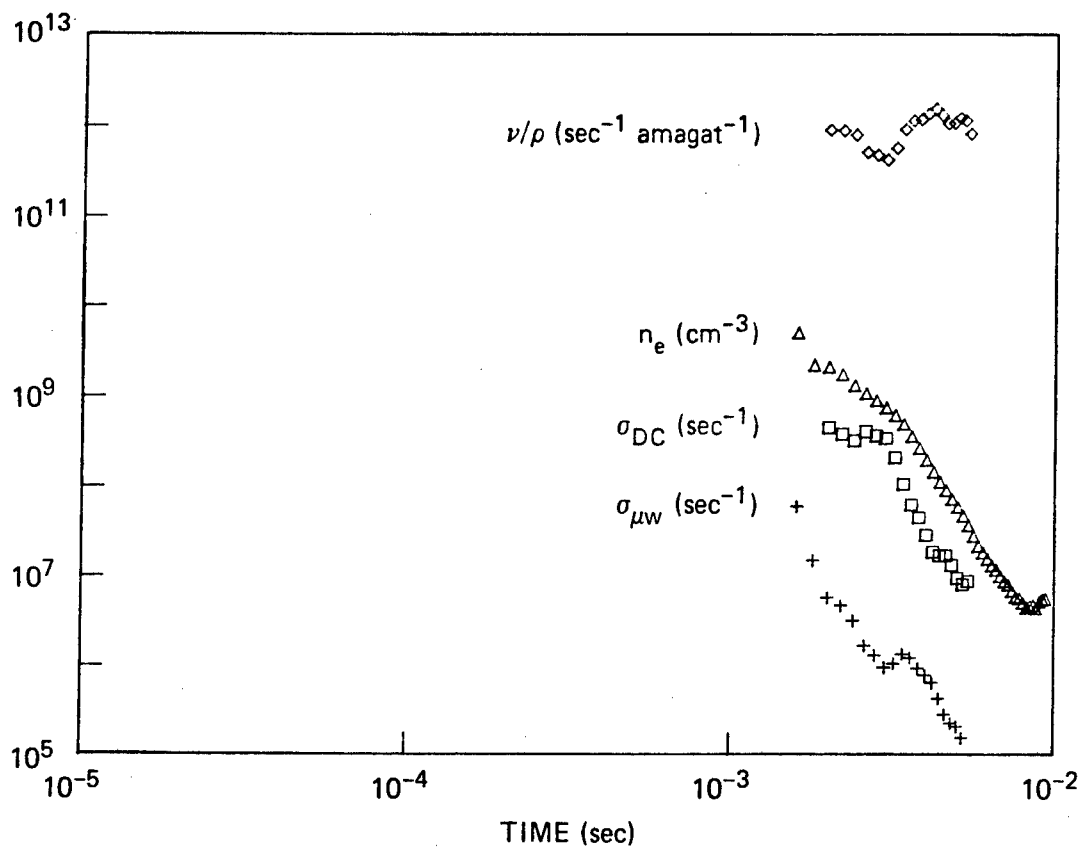
JA-8606-1A

FIGURE 2 SCHEMATIC OF MICROWAVE CAVITY EXPERIMENTAL SETUP



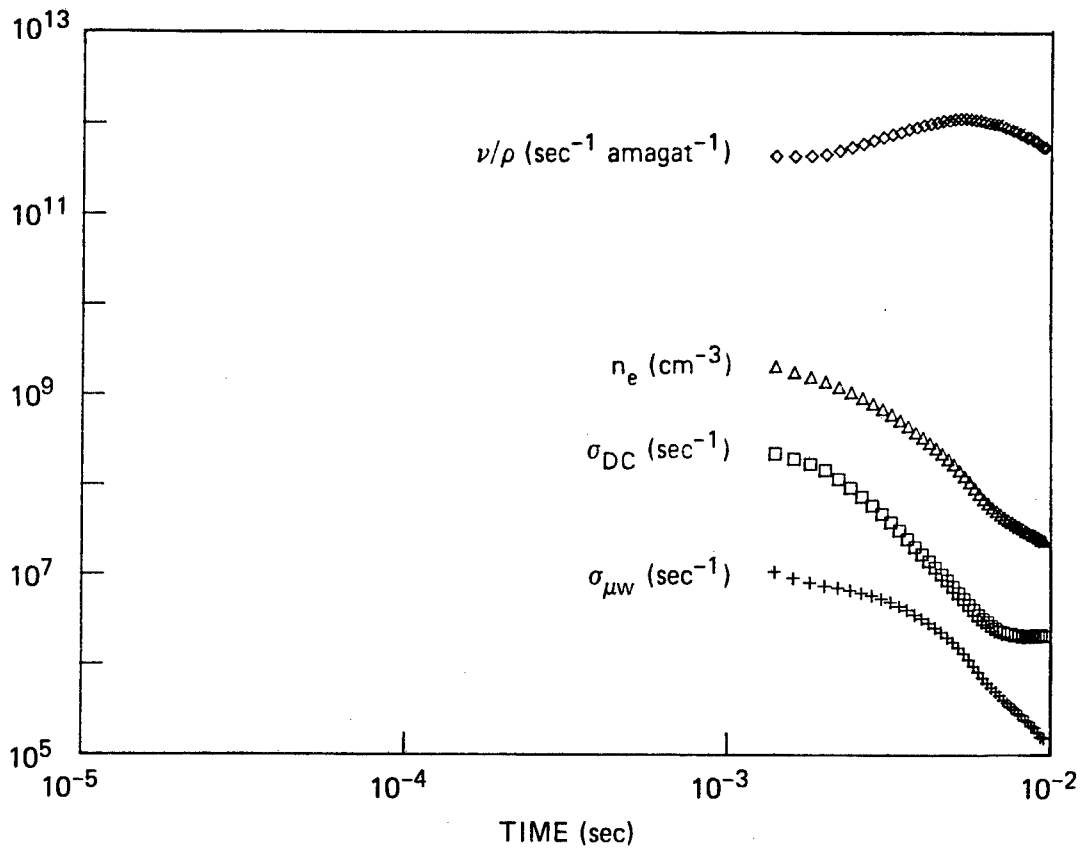
JA-8849-80

FIGURE 3 SCHEMATIC OF MICROWAVE INTERFEROMETER EXPERIMENTAL SETUP



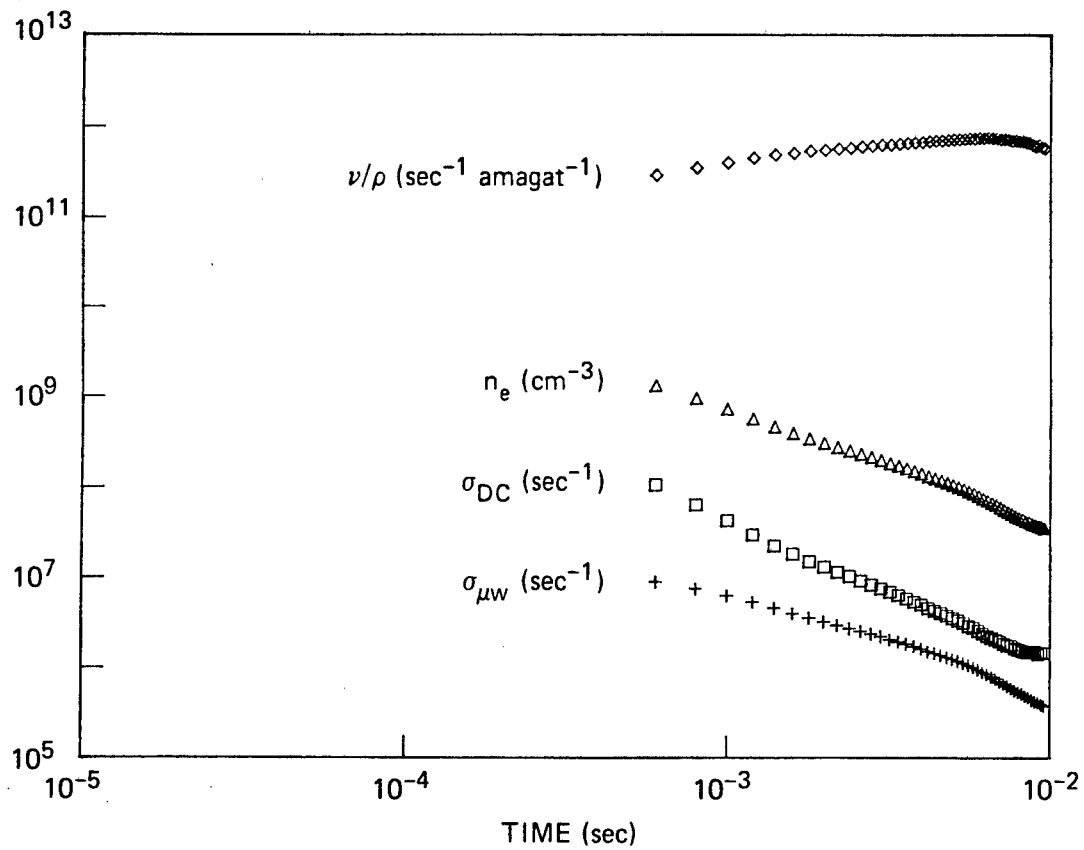
JA-8849-81

FIGURE 4 AFTERGLOW CONDUCTIVITY DECAY HISTORIES FOR 1-Torr SYNTHETIC AIR



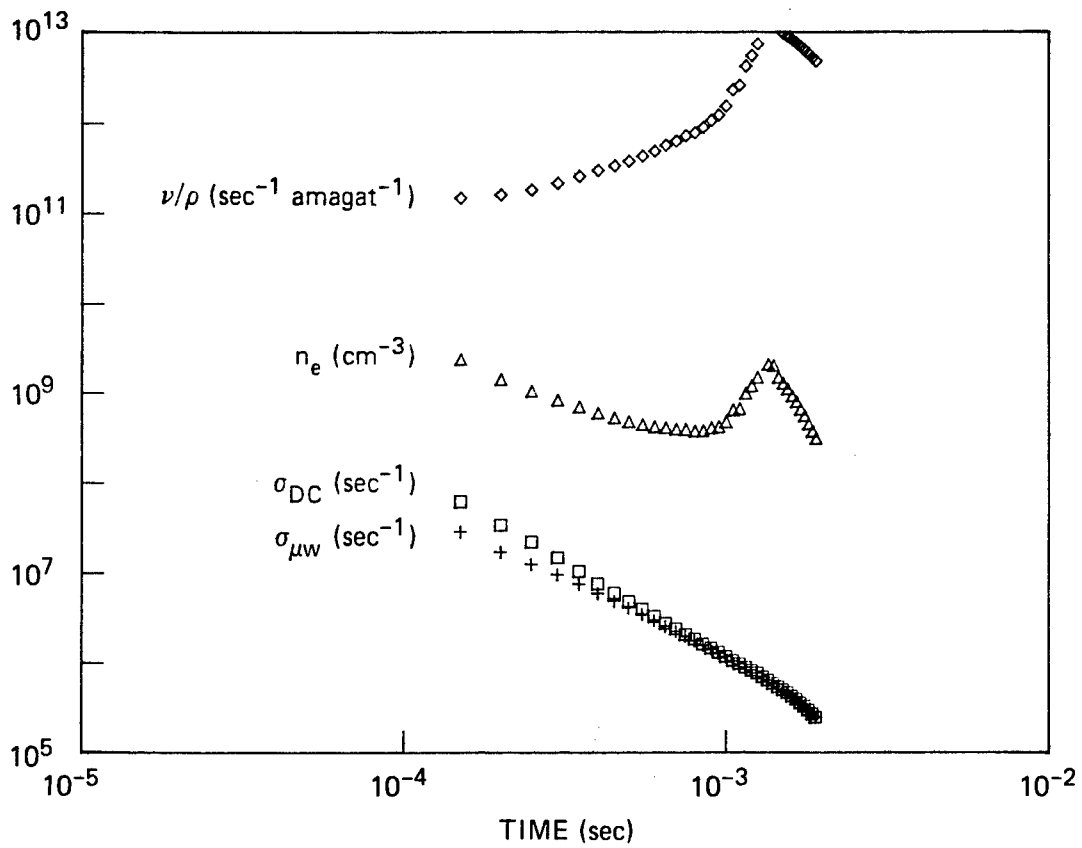
JA-8849-82

FIGURE 5 AFTERGLOW CONDUCTIVITY DECAY HISTORIES FOR 4-Torr SYNTHETIC AIR



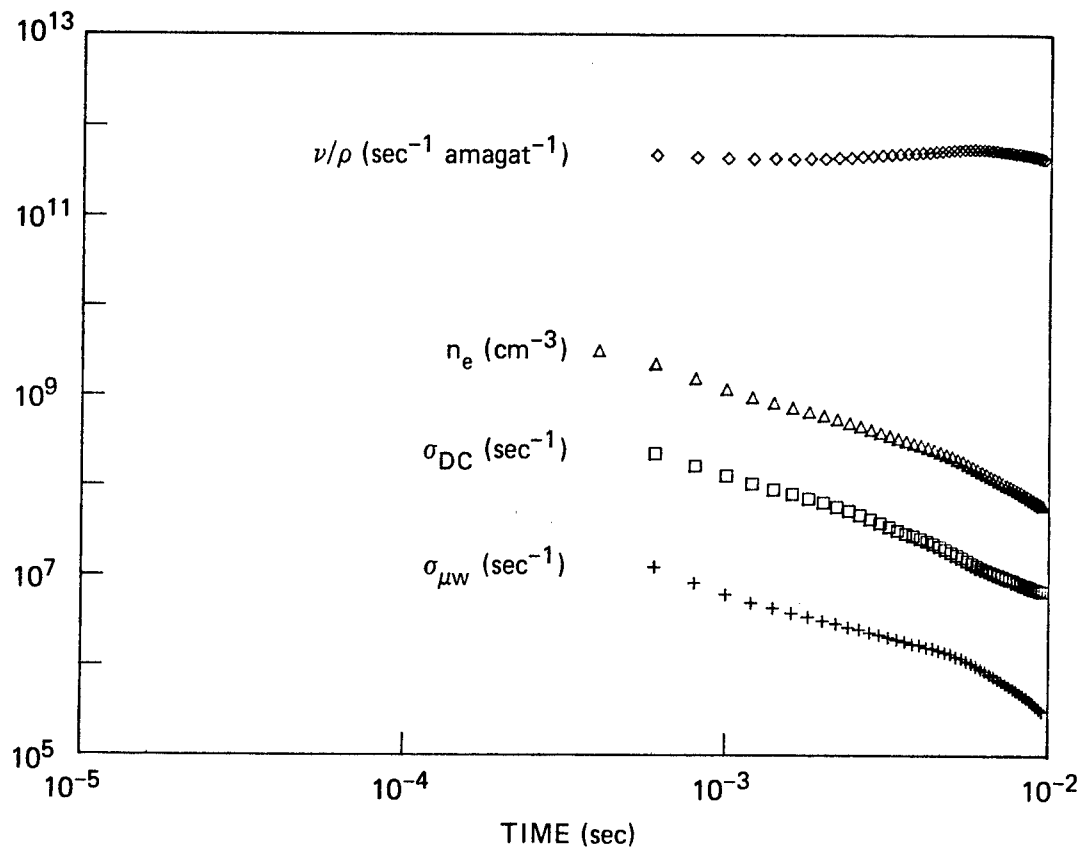
JA-8849-83

FIGURE 6 AFTERGLOW CONDUCTIVITY DECAY HISTORIES FOR 8-Torr SYNTHETIC AIR



JA-8849-85

FIGURE 8 AFTERGLOW CONDUCTIVITY DECAY HISTORIES FOR 50-Torr SYNTHETIC AIR



JA-8849-86

FIGURE 9 AFTERGLOW CONDUCTIVITY DECAY HISTORIES FOR 4-Torr LABORATORY AIR

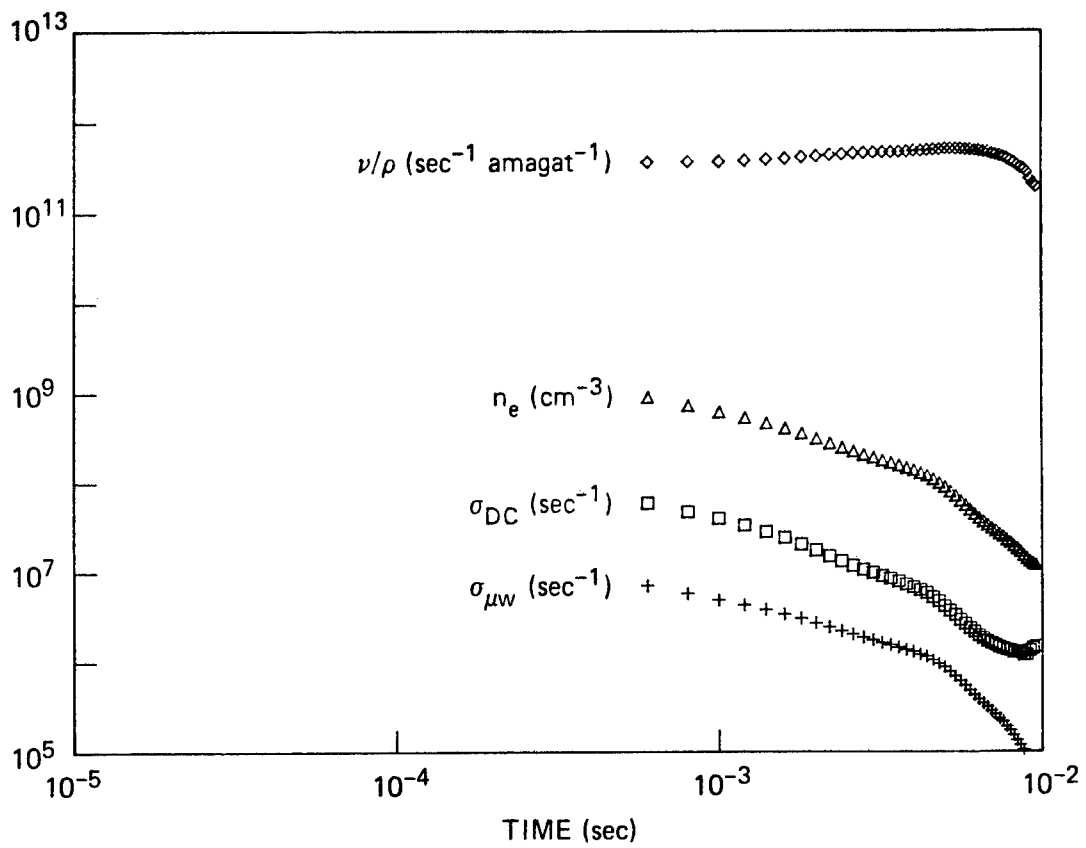
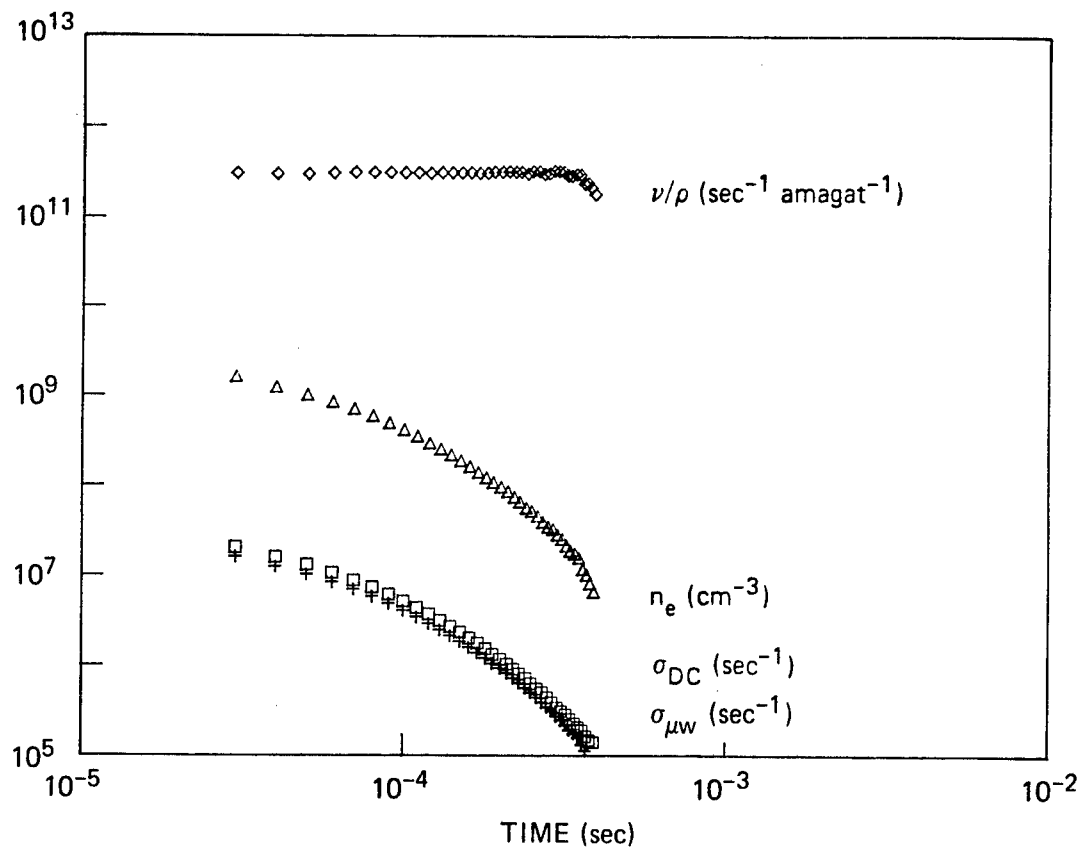
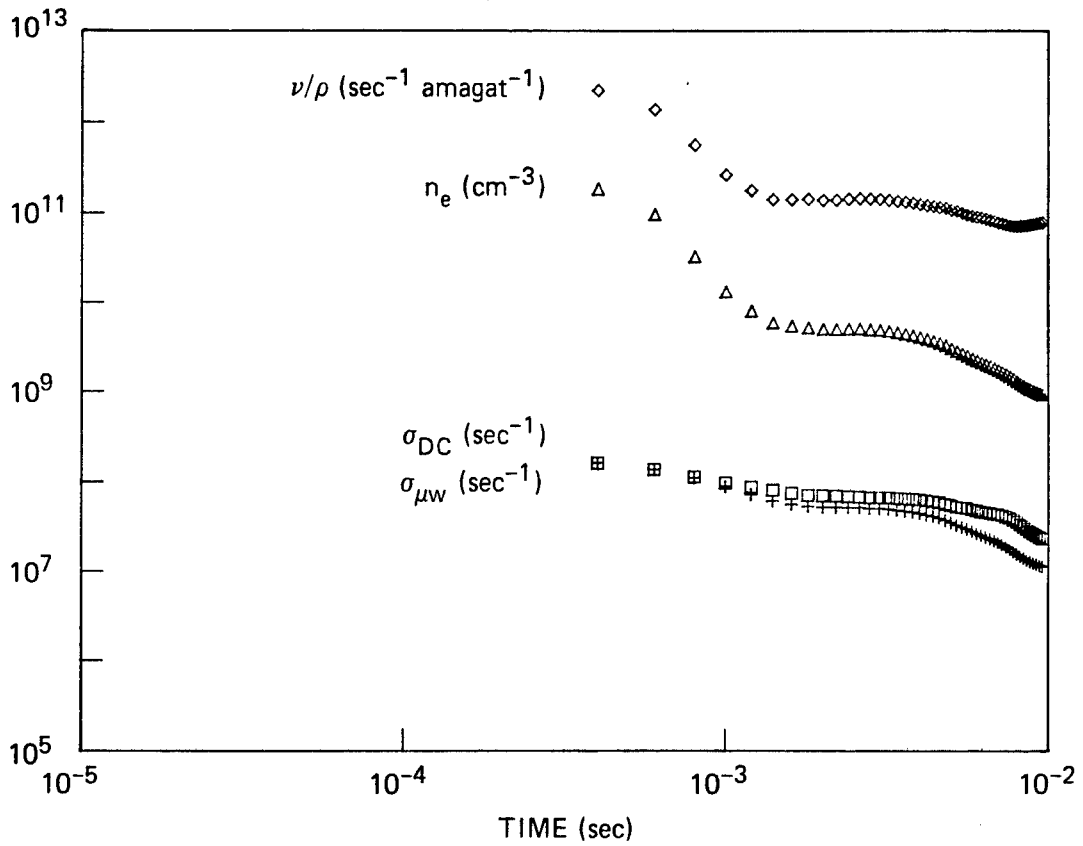


FIGURE 10 AFTERGLOW CONDUCTIVITY DECAY HISTORIES FOR 8-Torr LABORATORY AIR



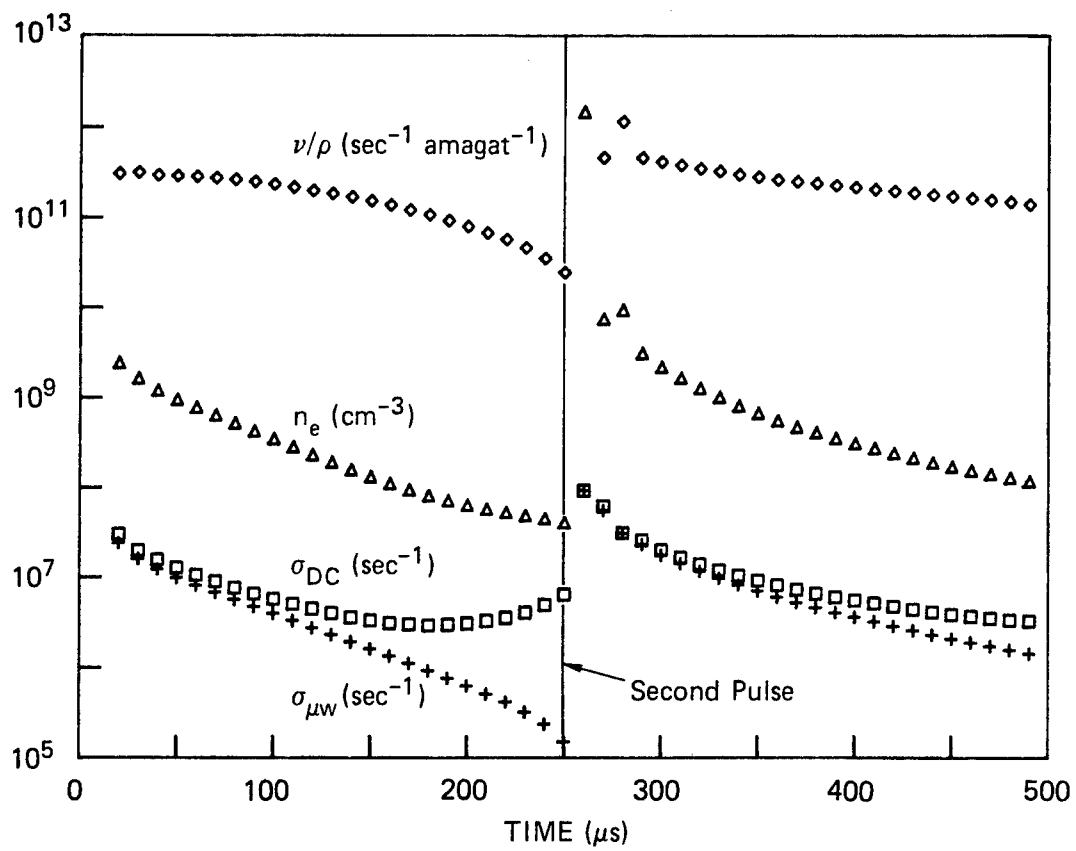
JA-8849-89

FIGURE 12 AFTERGLOW CONDUCTIVITY DECAY HISTORIES FOR 50-Torr LABORATORY AIR



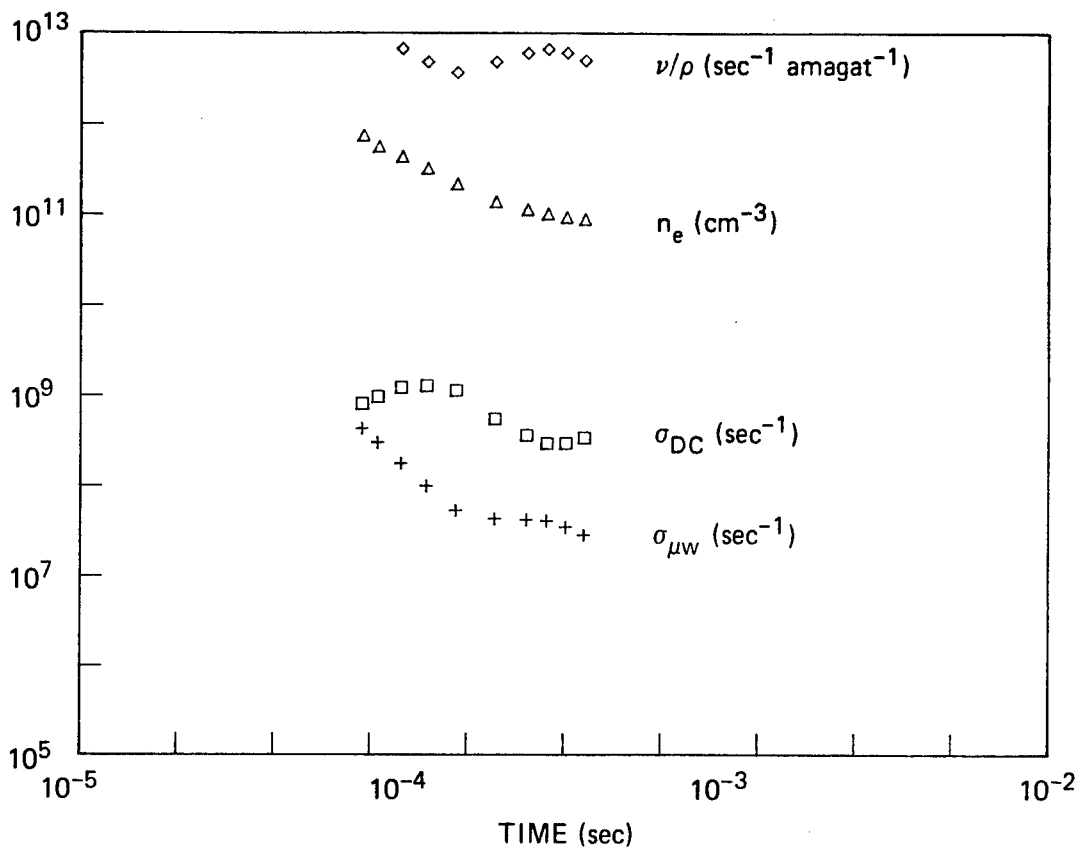
JA-8849-90

FIGURE 13 AFTERGLOW CONDUCTIVITY DECAY HISTORIES FOR 100-Torr NEON



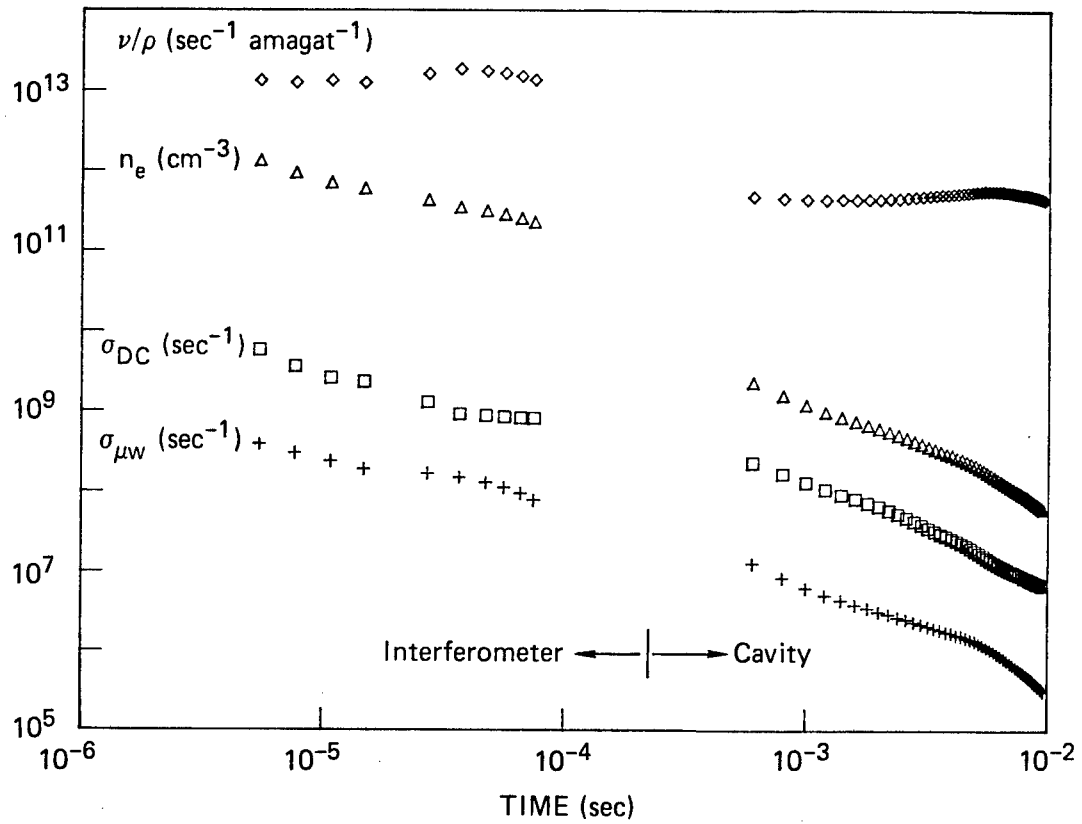
JA-8849-91

FIGURE 14 DOUBLE-PULSE AFTERGLOW CONDUCTIVITY DECAY HISTORIES FOR 50-Torr LABORATORY AIR



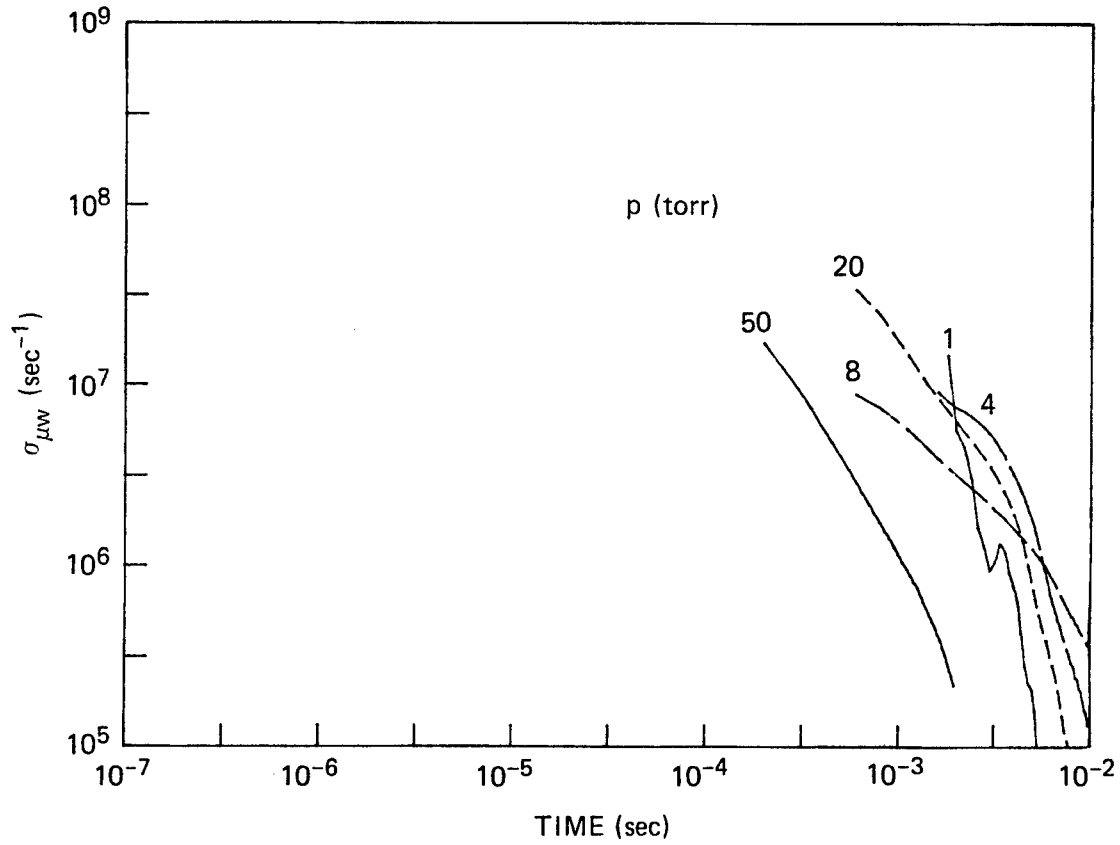
JA-8849-92

FIGURE 15 AFTERGLOW CONDUCTIVITY DECAY HISTORIES FOR 1-Torr LABORATORY AIR FROM INTERFEROMETER MEASUREMENTS



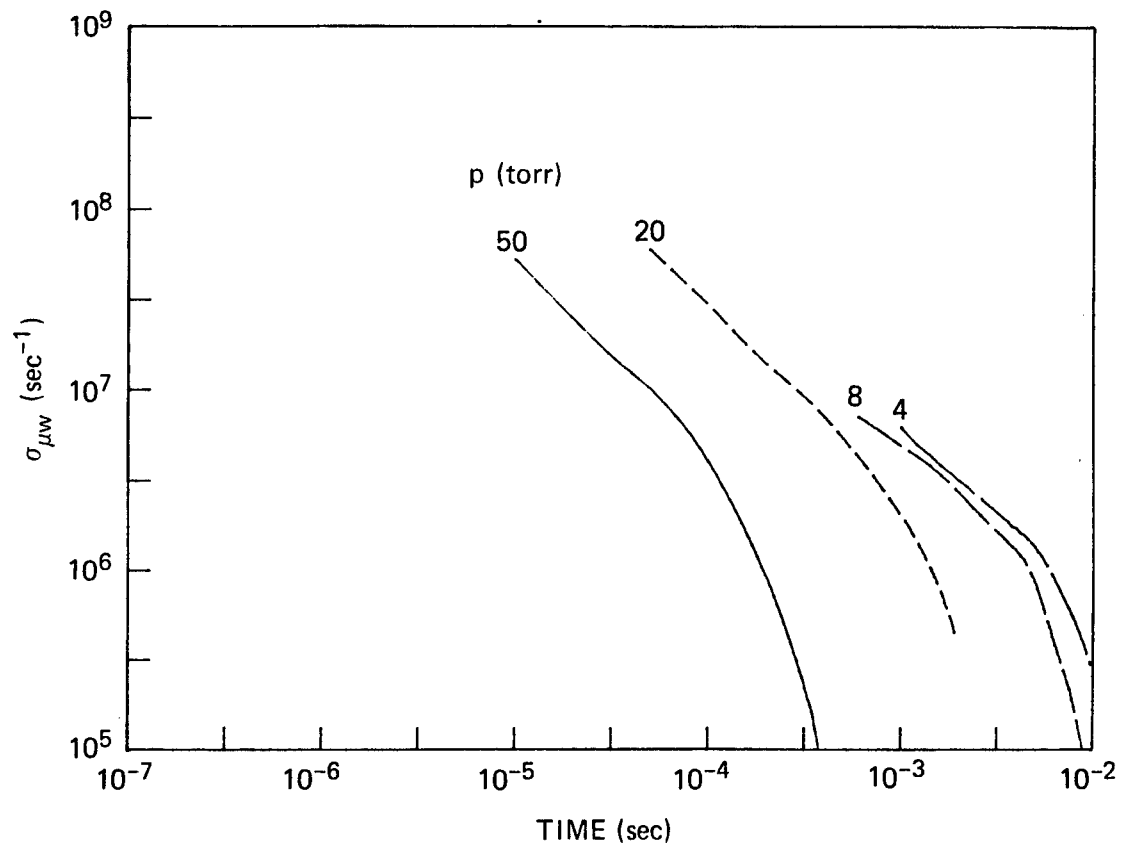
JA-8849-93

FIGURE 16 AFTERGLOW CONDUCTIVITY DECAY HISTORIES FOR 4-Torr LABORATORY AIR INCLUDING INTERFEROMETER DATA



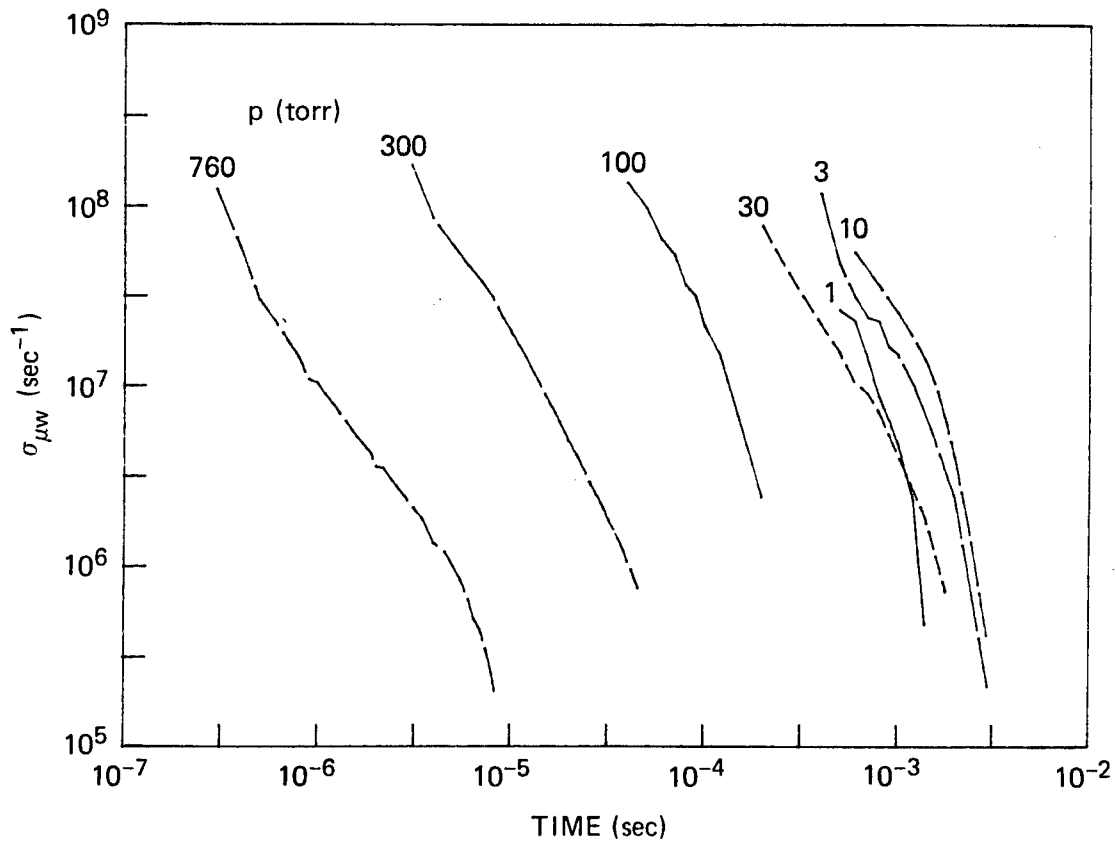
JA-8849-94

FIGURE 17 REAL CONDUCTIVITY HISTORIES FOR SYNTHETIC AIR EXCITED BY THE MEDEA ELECTRON BEAM



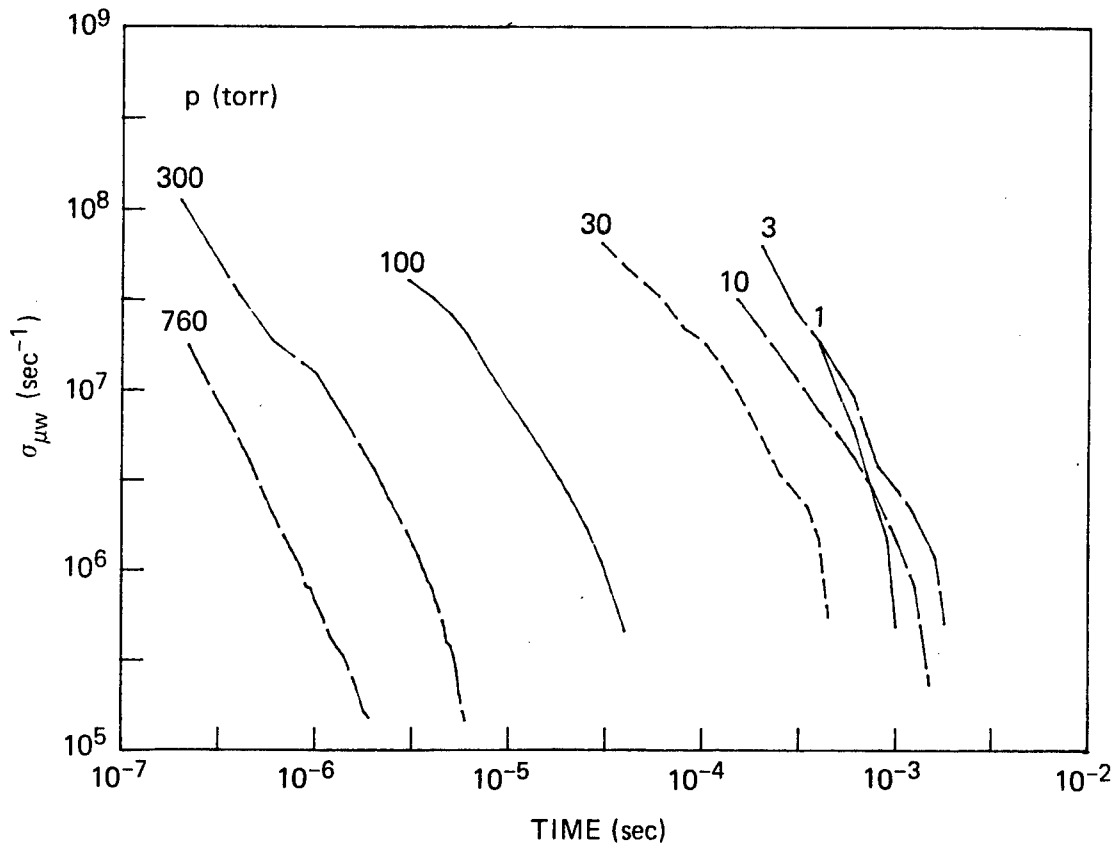
JA-8849-95

FIGURE 18 REAL CONDUCTIVITY HISTORIES FOR LABORATORY AIR EXCITED BY THE MEDEA ELECTRON BEAM



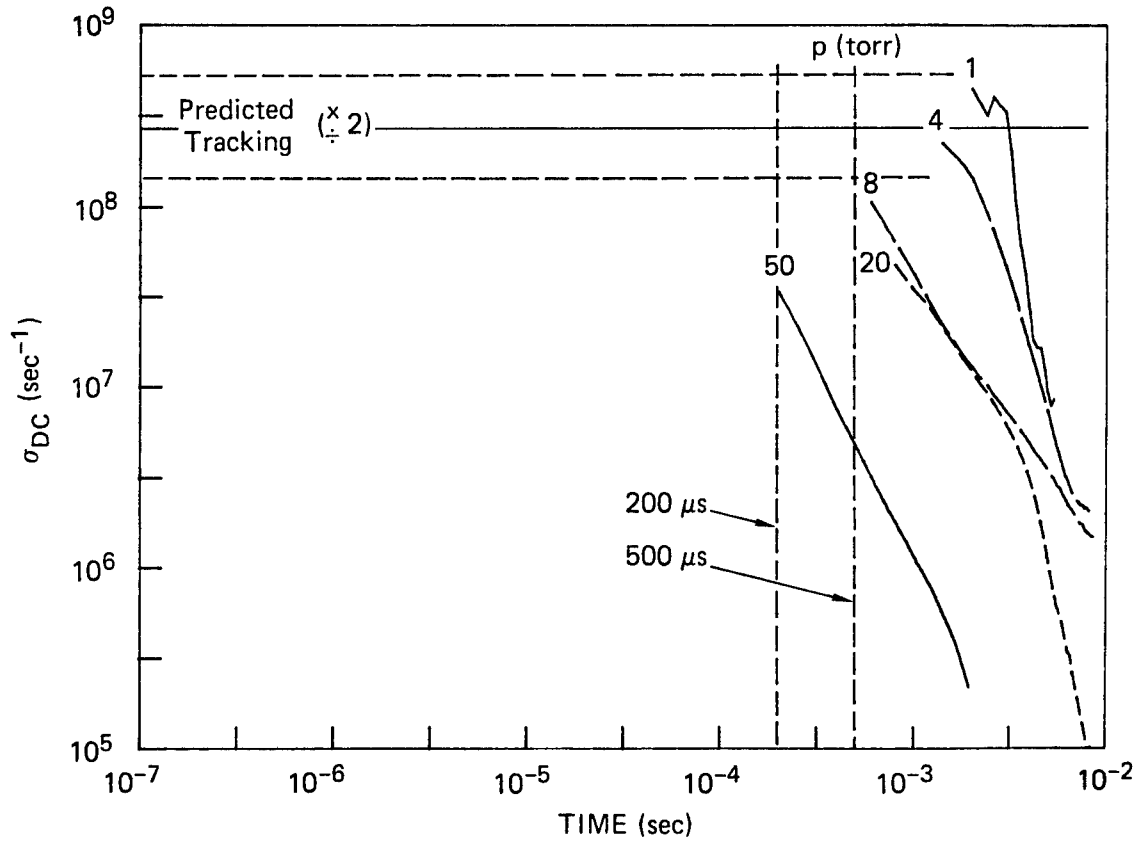
JA-8849-96

FIGURE 19 REAL CONDUCTIVITY HISTORIES FOR SYNTHETIC AIR EXCITED BY THE FEBETRON ELECTRON BEAM



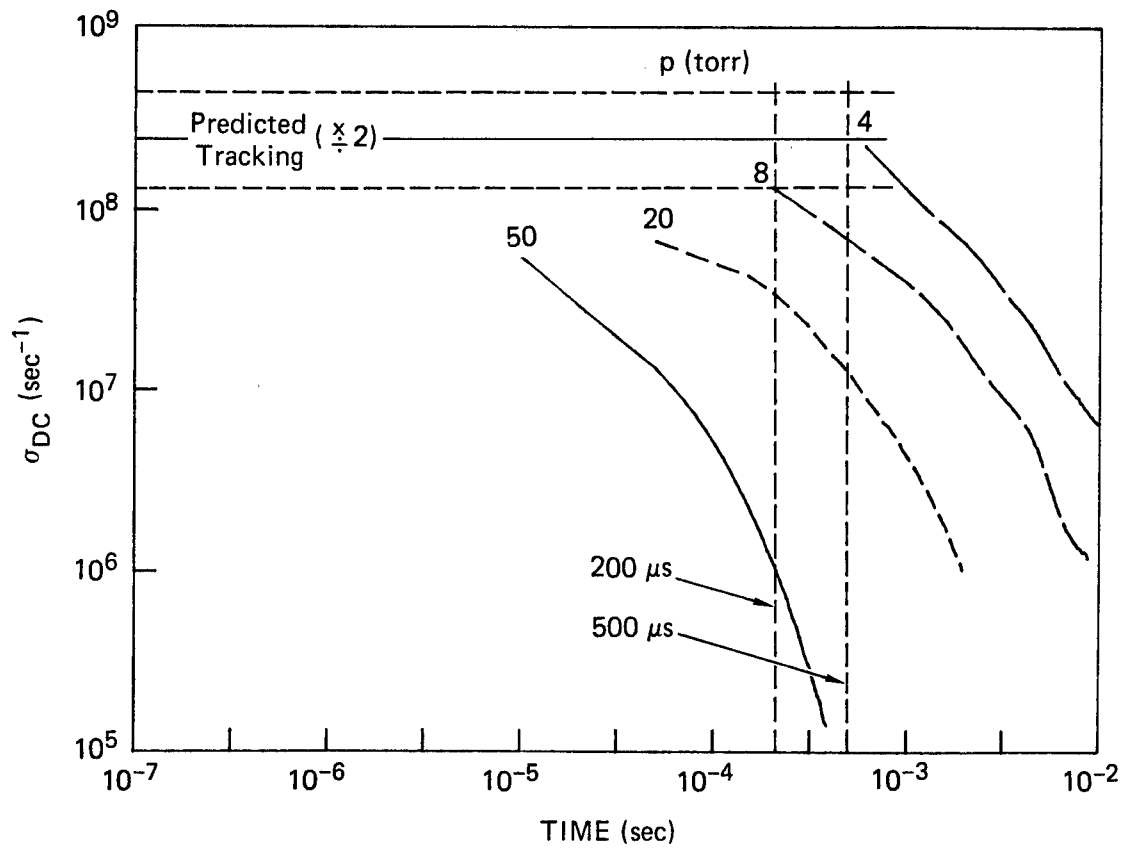
JA-8849-97

FIGURE 20 REAL CONDUCTIVITY HISTORIES FOR LABORATORY AIR EXCITED BY THE FEBETRON ELECTRON BEAM



JA-8849-98

FIGURE 21 D. C. CONDUCTIVITY HISTORIES FOR SYNTHETIC AIR EXCITED BY THE MEDEA ELECTRON BEAM



JA-8849-99

FIGURE 22 D. C. CONDUCTIVITY HISTORIES FOR LABORATORY AIR EXCITED BY THE MEDEA ELECTRON BEAM

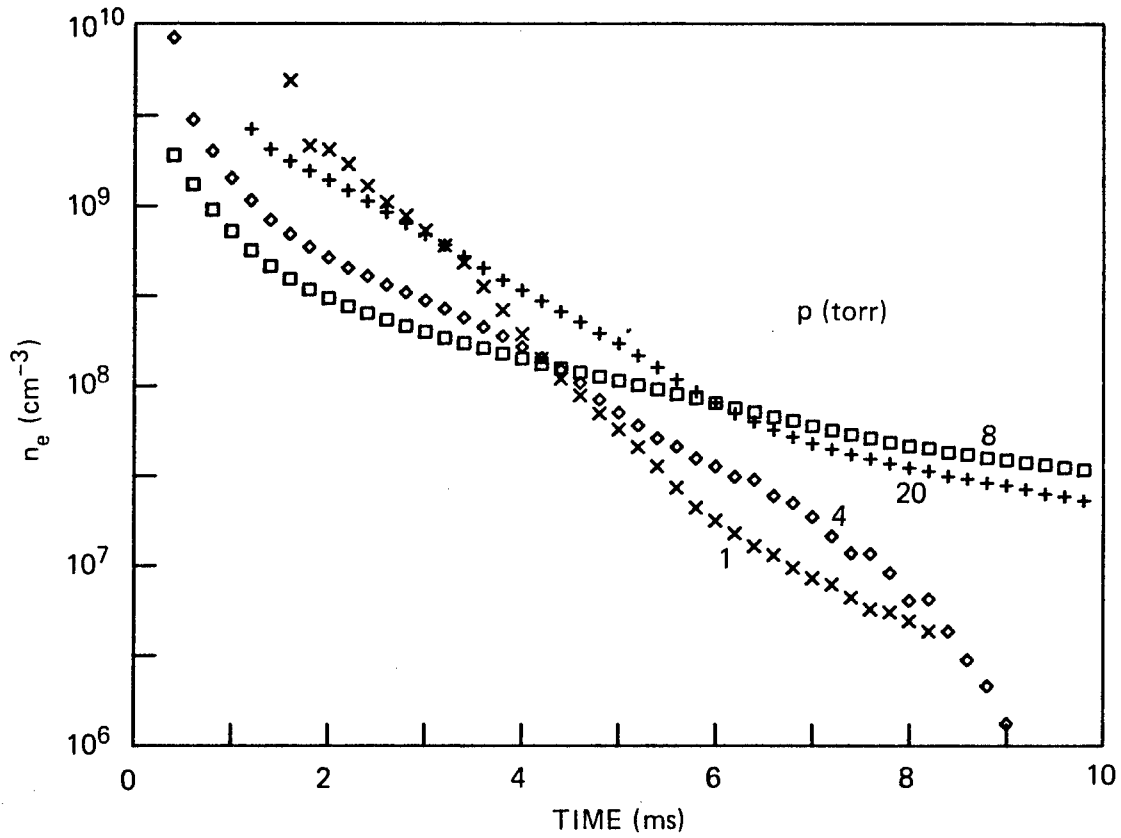


FIGURE 23 ELECTRON DENSITY HISTORIES FOR SYNTHETIC AIR EXCITED BY THE MEDEA ELECTRON BEAM

JA-8849-100

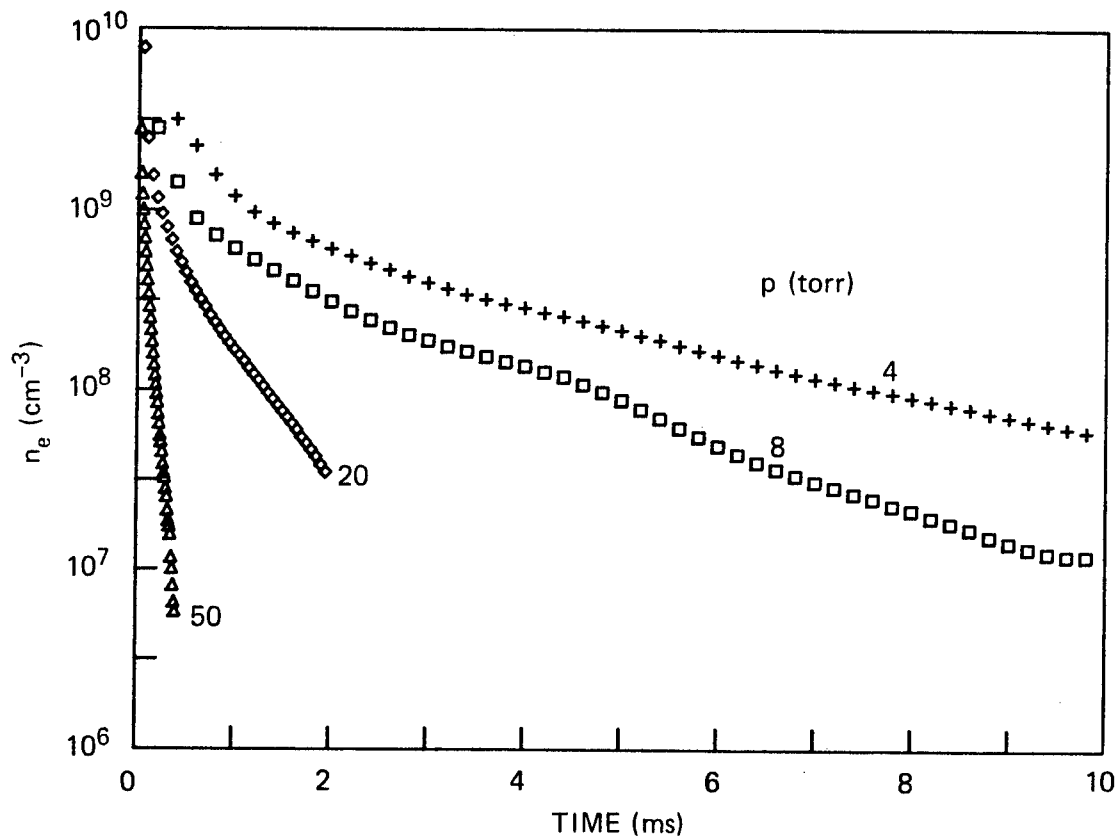
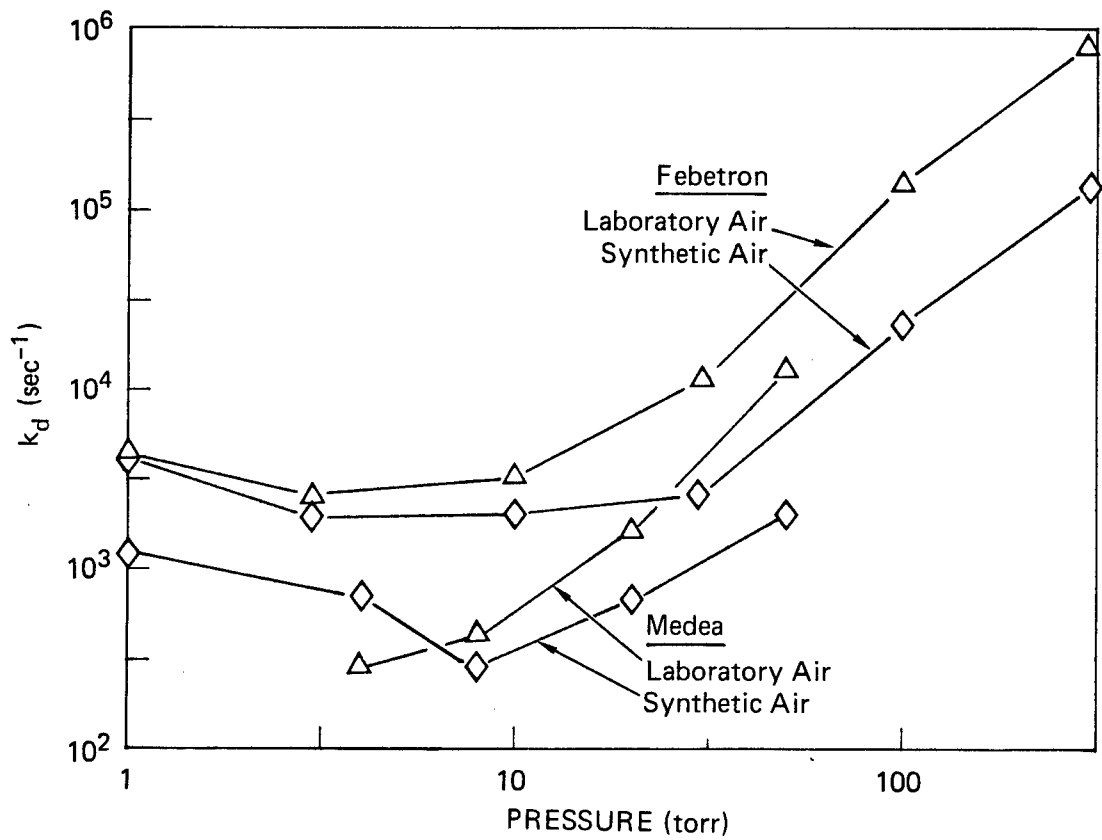
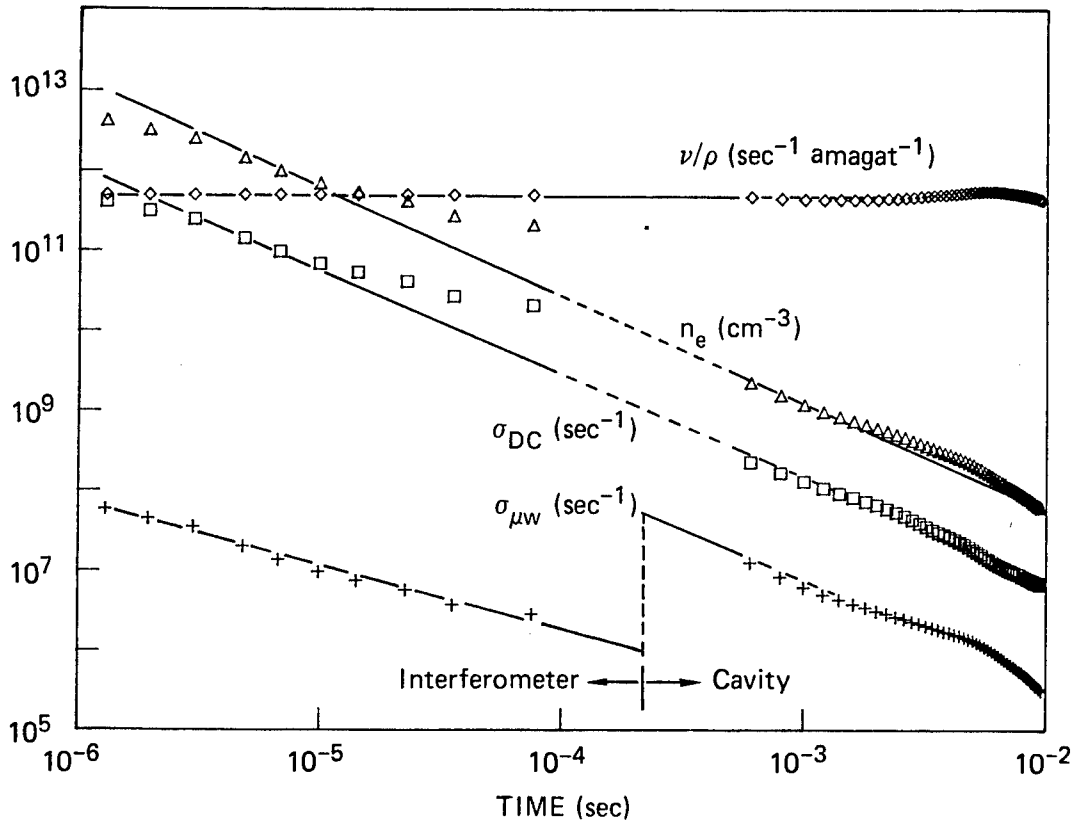


FIGURE 24 ELECTRON DENSITY HISTORIES FOR LABORATORY AIR EXCITED BY THE MEDEA ELECTRON BEAM



JA-8849-102

FIGURE 25 ELECTRON DENSITY DECAY RATES IN E-BEAM-EXCITED AIR



JA-8849-103

FIGURE 26 AFTERGLOW CONDUCTIVITY DECAY HISTORIES FOR 4-Torr LABORATORY AIR WITH CORRECTED INTERFEROMETER DATA